LAPPEENRANTA UNIVERSITY OF TECHNOLOGY
LUT School of Energy Systems
LUT Mechanical Engineering
Laboratory of Steel Structures

Tomi Suksi

STRESSES OF A BOAT TRAILER

Examiners: Professor Timo Björk
M.Sc Marko Haapakoski

ABSTRACT

Lappeenranta University of Technology
LUT School of Energy Systems
LUT Mechanical Engineering
Laboratory of Steel Structures

Tomi Suksi

Stresses of a boat trailer

Master's thesis

2015

66 pages, 31 pictures, 17 tables and 5 appendixes

Examiners: Prof. Timo Björk
M. Sc. Marko Haapakoski

Keywords: Finite element analysis, Strain gage measurement, Fatigue, Effective notch stress approach, Structural hot spot stress approach

In this thesis work, a strength analysis is made for a boat trailer. The studied trailer structure is manufactured from Ruukki's structural steel S420. The main focus in this work is in the trailer's frame.

The investigation process consists two main stages. These stages are strain gage measurements and finite elements analysis. Strain gage measurements were performed to the current boat trailer in February 2015. Static durability and fatigue life of the trailer are analyzed with finite element analysis and with two different materials. These materials are the current trailer material Ruukki's structural steel S420 and new option material high strength precision tube Form 800. The main target by using high strength steel in a trailer is weight reduction. The applied fatigue analysis methods are effective notch stress and structural hot spot stress approaches. The target of these strength analyses is to determine if it is reasonable to change the trailer material to high strength steel.

The static strengths of the S420 and Form 800 trailers is sufficient. The fatigue strength of the Form 800 trailer is considerably lower than the fatigue strength of the S420 trailer. For future research, the effect of hot dip galvanization to the high strength steel has to be investigated. The effect of hot dip galvanization to the trailer is investigated by laboratory tests that are not included in this thesis.

TIIVISTELMÄ

Lappeenrannan teknillinen yliopisto
LUT School of Energy Systems
LUT Kone
Teräsrakenteiden laboratorio

Tomi Suksi

Venetrailerin jännitykset

Diplomityö

2015

66 sivua, 31 kuvaa, 17 taulukkoa and 5 liitettä

Tarkastajat: Prof. Timo Björk
DI Marko Haapakoski

Hakusanat: Elementtimenetelmä, venymäliuskamittaus, väsyminen, tehollisen lovijännityksen menetelmä, rakenteellisen hot spot-jännityksen menetelmä

Tässä diplomityössä suoritetaan lujuusanalyysi venetrailerille. Tutkittava traileri on valmistettu Ruukin S420 rakenneteräksestä.

Työ koostuu venymäliuskamittauksista ja FE-analyysista. Venymäliuskamittaukset suoritettiin nykyiselle trailerille helmikuussa 2015. Traileria tutkitaan sen staattisen kestävyyden ja väsymisen kannalta kahdella eri materiaalilla. Vertailtavat materiaalit ovat trailerin nykyinen materiaali S420 rakenneteräs ja lujasta teräksestä valmistettu Form 800-ohutseinämäputki. Lujaa terästä käyttämällä pyritään vähentämään trailerin rungon massaa. Väsymiskestävyyttä tutkitaan tehollisen lovijännityksen menetelmällä ja rakenteellisen hot spot-jännityksen menetelmällä. Lujuusanalyysien pohjalta pyritään saamaan käsitys siitä, onko trailerin materiaalia kannattavaa vaihtaa.

Trailerin staattinen kestävyys on riittävä S420 ja Form 800 materiaaleilla. Form 800 ohutseinämäputkella valmistetun trailerin väsymiskestävyys työssä käytetyillä profiileilla on huomattavasti heikompi kuin S420 trailerin väsymiskestävyys. Jatkotutkimuskohteena kuumasinkityksen vaikutus lujan teräksen väsymiskestävyyteen trailerissa on tutkittava, ennen kuin päätös lujan teräksen käytöstä trailerissa voidaan tehdä. Kuumasinkityksen vaikutusta traileriin tutkitaan väsytyskokeilla, jotka eivät sisälly tähän työhön.

ACKNOWLEDGEMENTS

Honorable mentions to the LUT Laboratory of Steel Structures for providing me this interesting thesis, which increased my knowledge and skills in the field of steel structures. Thanks to Professor Timo Björk from Lappeenranta University of Technology, who supervised me and advised me with his knowledge. Thanks also for the cooperation to all of the members of APGASS, especially to Marko Haapakoski from Majava and to Jussi Minkkinen from SSAB. Thanks to TEKES/Fimecc-project and BSA-project for financing this project and to Vesa Järvinen from Unisigma for performing the strain gage measurements.

Thanks to my family for the support along the way.

Tomi Suksi
Lappeenranta, August of 2015

TABLE OF CONTENTS

APPENDIXES

LIST OF SYMBOLS

A	Area [mm^2]
E	Modulus of elasticity [MPa]
e_o	Output voltage [U]
F	Axial force [N]
f_y	Yield strength [MPa]
ε	Engineering strain [mm]
k	Gage factor [-]
$R_{A,B,C,D}$	Resistances of strain gages [Ω]
U	Output voltage [U]
M	Bending moment [Nm]
m	The slope of S-N curve [-]
N	Load cycles [-]
$N_{Form\ 800}$	Fatigue life of Form 800 trailer in relation to S420 trailer [-]
n	Amount of stress cycles [-]
$t_{Form\ 800}$	Thickness of Form 800 profile [mm]
t_{S420}	Thickness of S420 profile [mm]
V	Input voltage [U]
v	Poisson's ratio [-]
W	Section modulus [mm^3]
σ	Stress [MPa]
$\Delta\sigma$	Stress change [MPa]
$\sigma_{0,4t}$	Stress at the distance of 0.4·t from the weld toe [MPa]
$\sigma_{1,0t}$	Stress at the distance of 1,0·t from the weld toe [MPa]
σ_{eff}	Effective notch stress [MPa]
$\sigma_{eff,eqv}$	Equivalent effective notch stress [MPa]
σ_{hs}	Hot spot stress [MPa]
$\sigma_{hs,eqv}$	Equivalent hot spot stress [MPa]

ABBREVIATIONS

ENS	Effective notch stress approach
FAT	Fatigue class
FEA	Finite element analysis
LME	Liquid metal embrittlement

1 INTRODUCTION

The use of high strength structural steels in trailer industry is minor and the advantages of this steel class are not exploited in trailer structures. The advantages of high strength steels have nowadays come to wider knowledge and the interest towards this steel class has grown. One great advantage by using high strength steels is the weight reduction that can be achieved by using them.

The target of this thesis work is to perform a strength analysis to a boat trailer. The other main target is to determine, if it is reasonable to change the material of the trailer to high strength steel in order to achieve weight reduction from the frame. The main focus in this work is in the trailer's frame, thus consequently for example the tires and suspensions are not under investigation.

The strength analysis includes strain gage measurements and finite element analyses (FEA) by using Femap and Abaqus softwares. Medial surface modeling is performed using Femap and closer solid element modeling is performed with Abaqus. The materials applied in this work are Ruukki's S420 structural steel and Form 800 high strength rectangular precision tube. The current trailer is manufactured from S420 structural steel.

The analyzing process begins with measurement plan for the strain gage measurements. For the measurement plan, a simple medial surface FE-model is made and the critical locations of structure are located. From the results of strain gage measurements the actual loadings can be determined and the trailer can be analyzed properly with FEA. Static and fatigue analyses are performed with FEA. Fatigue calculations are performed with effective notch stress approach and with hot spot stress approach for the most critical location of the structure. At the end, comparison is made between these two approaches and the one that suits better for this kind of structure will be chosen. After these analyses it is presented if the use of high strength steel in the boat trailer is reasonable.

2 MATERIALS

The materials applied in this work are Ruukki's structural steel S420 and high strength precision rectangular tube Form 800. The current boat trailer is manufactured from the S420 structural steel. Because of the need of lighter and economical solution for the trailer, Form 800 is considered to be a new alternative to be used in trailer's frame. The use of high strength steels in the trailer frame would be a great advantage in the markets and it is something that is never before applied in the trailers. Form 800 precision tubes are manufactured from dual phase or high strength steel alloys. (Table 1.)

Table 1. Mechanical properties and chemical compositions of used materials (Ruukki, 2014).

	S420 structural steel	**Form 800 precision tube**
	Cold-rolled	
Yield strength $R_{p0.2}$ (MPa)	420	600
Tensile strength R_m (MPa)	500-660	800
Elongation A_5 (%)	19	10
C, content weight (%)	0.08	0.15
Si, content weight (%)	0.18	0.3
Mn, content weight (%)	1.4	1.6
P, content weight (%)	0.01	-
S, content weight (%)	0.006	-

In Finland, welded profiles are usually made from S355 structural steel, which can be considered to be as basic strength steel. In Eurocode, S420 and S460 are also considered as low and mild strength steels and these strengths are also widely used. Steels that have higher strength are considered as high strength structural steels. Steels that have greater strength than S460 are slightly used in industry because of the lack of good designing instructions. In recent years, the prices of high strength steels have decreased significantly and are nowadays competitive against the low and mild strength steels. In figure 1 is presented relative price for sheet metal in year 2007. (Ruukki, 2010, p. 45.)

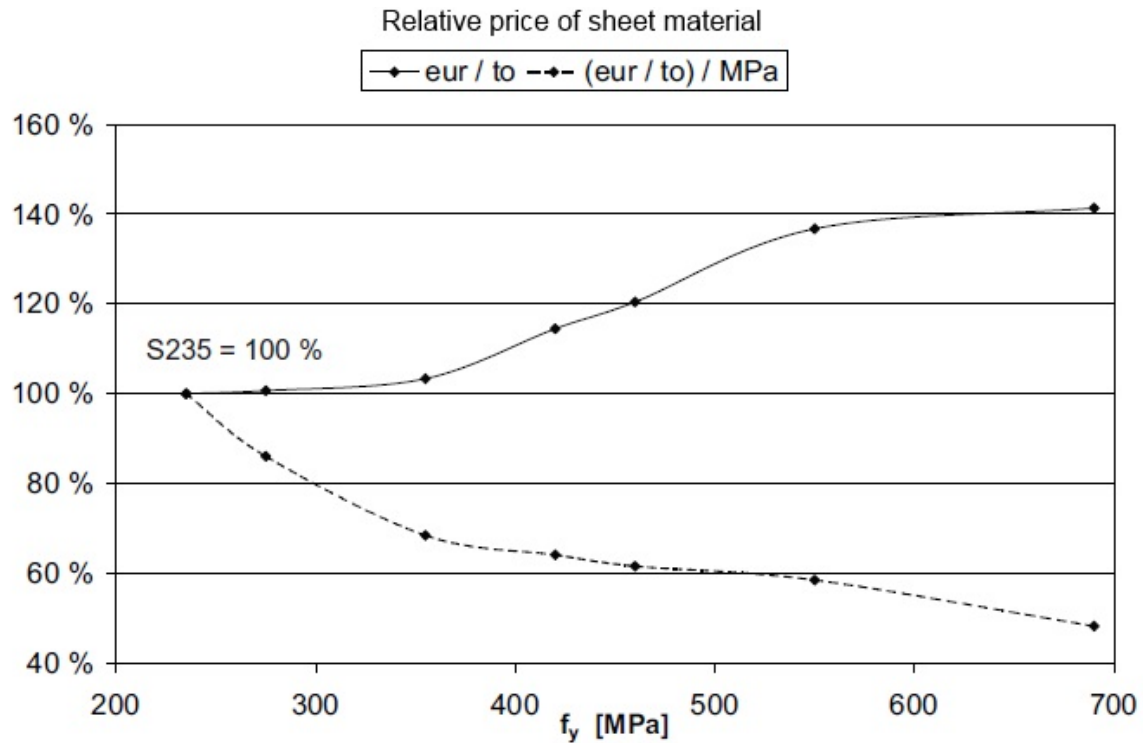

Figure 1. S235-S700 sheet material prices in 2007 in relation to S235 price. Euros per ton. (Ruukki, 2010, p. 45.)

In practice it is hard to exploit all the advantages of high strength steels especially when a great weight reduction is striven. There are also restrictions in Eurocode, which can make the use of these high strength steels complicated. The use of high strength steels affect directly to manufacturing costs. Profile thicknesses are likely to be thinner, which affect for example the welding process. Welding may need some special arrangements, which are not needed when using mild strength steels. On the other hand, handling of the part might be easier and the need of additive in welding process will be smaller. (Björk, 2015; Ruukki, 2010, p. 46-47.)

The fatigue life for as-welded joints in structures consists mainly of the crack initation stress cycles. The crack growth rate does not depend from the steels grade or the welds properties. It means that the fatigue life for high strength steels is the same as for low and mild strength steels. If structure's weight reduction is attempted to achieve by using high strength steels it will lead to greater stress changes and faster crack growth, which will lead to shorter fatigue

life. Consequently, the only way to to exploit the high strength steels in terms of better fatigue life is to improve the quality of the weld on the level, where the crack initiation is a remarkable period in the total fatigue life of the joint. (Björk, 2015; Niemi et al., 2004, p. 10.)

One of the goals of this work is to achieve weight reduction in the trailer's frame by using high strength steels. This goal requires that there is a chance to take thinner profile thicknesses into account.

2.1 Ultra-high strength and high strength structural steels

High strength steels are used for structures in many countries because of their many advantages. Also ultra-high strength structural steels are widely used. Many differences can be found between the high strength structural steels and the low and mild strength structural steels. These differences are for example residual stress distribution and stress-strain curves, which have a significant effect to mechanical performance of steel members. Ordinary steels are well studied and there are good specifications of how structures need to be designed when using these steels. Ultra-high strength and high strength structural steels are not so well studied. For example, there is not much information about the buckling behavior of high strength structural steels. (Gang, Huiyong & Bijlaard, 2012, p. 237; Wei, 2013, p. 141-150; Ilvonen et al., 2008, p. 30-35.)

By end users, particularly the transport section is constantly targeting to weight reduction, increase of safety and performance to get along in the tough competition in the industry. High strength structural steels that have a good weldability and formability is increasingly noticed to be a good way to achieve those targets. Car industry and bridges industry has successfully used tempered and quenched steels with yield strengths over 740 MPa. For high strength steels and mild steels the Young's modulus is the same. That will lead to decreasing of stiffness when material thickness is reduced. Changing the shape of the cross section can compensate this decreasing. (Sperle, 1997, p. 3-7)

According to Sperle (1997, p. 8) " When introducing high strength steels into fatigue loaded structures it is important to note that the fatigue strength of welded joints does not normally increase with the increasing base metal strength." The resistance for crack growth does not

distinguish when comparing high strength steels and mild steels. Same thing is with weld joints fatigue strength, it does not distinguish. For optimum performance of high strength steels with structures under fatigue loading, is to make sure that the welds locate in the areas where stresses are low. (Sperle, 1997, p. 8)

3 THEORETICAL STUDY

In this chapter theories behind the methods and processes considered in this work are presented. The main themes are fatigue, effective notch stress approach, hot spot stress approach, strain gage measurement, hot-dip galvanization and liquid metal embrittlement. The effects of hot-dip galvanization to the trailer's strength properties are not examined closer in this thesis. Possible consequences to the trailer due to galvanization process are presented in this chapter. It might affect greatly to the trailer's durability. The effect of hot-dip galvanization to the trailer is a future research project.

3.1 Hot-dip galvanization

Hot-dip galvanizing allows designing and building steel structures in sustainable and economic way. Optical and esthetical advantages resulting from the surface appearance makes hot-dip galvanization to a preferred selection alternative. Hot-dip galvanization is a technique, which protects iron and steel surfaces against corrosion. The technique is over 150 years old. In hot-dip galvanization the steel product is immersed in a liquid zinc bath for three to seven minutes. The bath is usually 450 degrees Celsius. This immersion causes chemical reactions between the zinc and the iron in the steel. Before the hot-dip galvanization can be performed, the steel must be cleaned properly. The stages of galvanization process are presented in Table 2 and figure 2. (Carpio et al., 2010, p. 19.)

Table 2. Hot-dip galvanization process (Suomen kuumasinkitsijät ry, 2007).

1.	Removing paint, dirt and grease from surfaces.
2.	Removing rust from the component.
3.	The component is washed with water.
4.	Fluxing.
5.	Drying.
6.	The component is immersed into molten zinc.
7.	Cooling down the component after zinc bath.
8, 9.	Inspections and weight measurements.

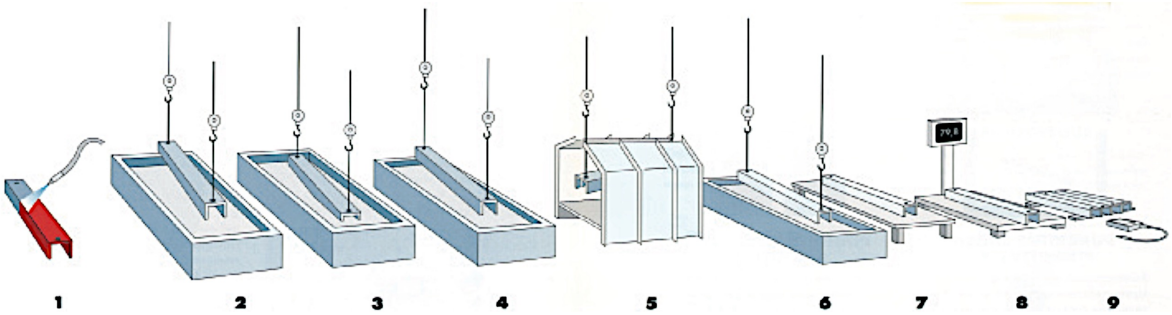

Figure 2. Hot-dip galvanization process (Suomen kuumasinkitsijät ry, 2007).

Occasionally cracks appear during the hot-dip galvanization of large steel components. Those cracks are covered with zinc and cannot usually be detected until the structure is subjected to loading or is inspected for the first time. This can be a large risk in structures that have high responsibility. (Carpio et al., 2010, p. 19)

3.2 Liquid metal embrittlement

Zinc coating can cause early structure failure especially under fatigue loading. Hot-dip galvanization process can cause cracks to bare steel when the liquid zinc touches it. This phenomenon is called liquid metal embrittlement and it can be critical especially for high strength steels. The phenomenon is quite much studied but there are many parameters that can vary for example material properties, geometry, residual stresses and the composition of the zinc bath so there is no absolute certainty of how the phenomenon progresses.

Liquid metal embrittlement (LME) is a phenomenon that manifests itself by the brittle fracture of ductile metal in the presence of stresses and liquid metal. LME is a catastrophic deterioration of the material's mechanical properties. It occurs within a limited temperature range. The lower temperature of this domain corresponds to the melting point of the embrittling metal. LME is also largely time independent and appears to depend only upon the liquid metal wetting the surface of the embrittled metal to operate. (Vidensky et al., 1998, p. 349.)

Cracks in the hot-dip galvanized coating form rapidly during cyclic loading and then propagate into the steel substrate. The crack initiation phase is therefore greatly shortened. Macroscopically the surfaces of galvanized and non-galvanized parts look the same. That prefers

that the crack initiation begin under the zinc surface, from the surface of the base material. The crack growth is strongly accompanied with the load ratio. Major factor is also the original structure, which might have some notches or cracks already in it. Also the cracks in the zinc coating might affect greatly, depending of the structure and the treatments that is made for it. With smaller stress changes, the difference in fatigue lives increases compared to great stress changes. Some test reports say that the decrease of fatigue strength is much greater for carbon steels than for tempered or annealed steels. This corresponds with the generally accepted idea that hard steels with low ductility are much more susceptible to notch effects compared to ductile and softer steels. (Björk, 2015; Feldmann, p. 214; Berchem et al., 2006, p. 598; Swanger et al., 1933, p. 18.)

Liquid metal embrittlement can be defined as a loss of ductility of a usually plastic material in the presence of liquid material. It has been discovered also that internal residual stresses, external loads, immersion time, specimens surface roughness, yield strength of steel and composition of zinc bath are necessary for LME to occur. Finding an explanation for the mechanisms of this LME phenomenon allows finding solution for many practical problems. For example as using the phenomenon to increase the efficacy of certain actions, such as reaming or crushing of very hard materials, or protection against destruction caused by contact of a stressed material with molten metal. The risk on LME has been confirmed but it is still difficult to describe it because of the lack of information and knowledge of the phenomenon. There seems to be also many parameters that are responsible for LME. (Mendala, 2012, p. 1-2; Kinstler, 2010, p. 66-71; Berchem et al., 2006, p. 597.)

Liquid metal embrittlement is a difficult phenomenon to research. It is invisible, so the problem is apparent only after the galvanization process and it is hard to determine when the crack has occurred. The phenomenon is rare, so there is no investigative protocol to preserve the samples. The phenomenon is also complex. It is hard to make any precautions, which might be expected to impact the phenomenon in positive or negative way. There are only few documents about the phenomenon and that is mainly because the galvanization process destroys evidences, which might be on the fracture surface for example concentrations of precipitates. (Kinstler, 2010, p. 66-71.)

3.3 Hydrogen embrittlement

Hydrogen embrittlement cracking is a critical problem with high strength structural steels, because it leads to a major decrease of structures mechanical properties, especially crack growth resistance. There are two different mechanisms known as internal hydrogen assisted cracking and hydrogen environment assisted cracking, which are also known as internal hydrogen embrittlement and hydrogen environment embrittlement. It is found in researches that hydrogen lowers the crack propagation resistance processes in steels. (Gangloff, 2003, p. 7-16.)

There are many metallurgical, mechanical and environmental variables that affect to internal hydrogen embrittlement and hydrogen environmental embrittlement in high strength alloys. Those variables are for example grain size, strength and purity. Also small crack size, application rate, stress intensity level, loading mode and the solution used in galvanization affect. Increasing or decreasing temperature in the process can eliminate effects of internal hydrogen embrittlement and hydrogen environmental embrittlement. (Gangloff, 2003, p. 169-172.)

3.4 Strain gage measurement

The strain gage measurement is used to find out the stress state of structure. The process does not actually measure the stress state of the structure but the voltage of the electric circuit. Variation in voltage is determined by the strain of the sensor. When measuring an object, the strain gage is glued to the examined object. The lattice experiences the same strain as the object. The strain of the grid is equivalent to the grid's voltage change, which is then measured. The strain gage system is presented in figure 3. (Hannah & Reed., 1993, p. 257.)

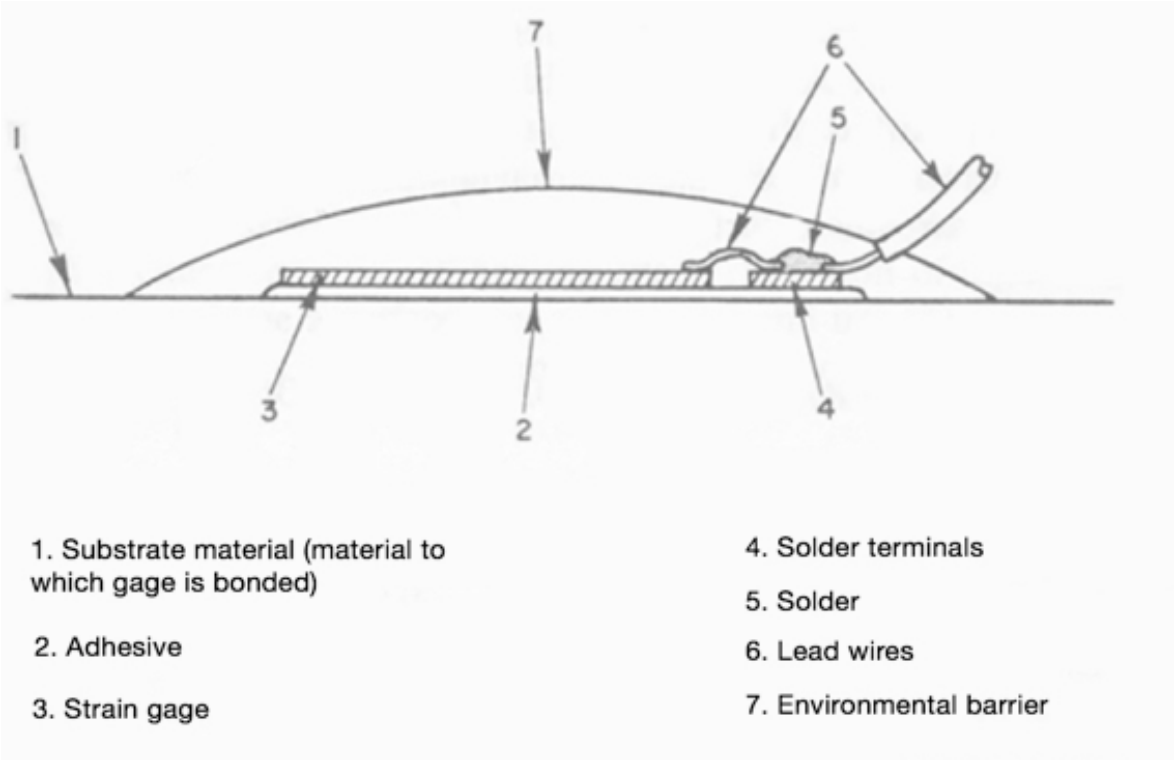

Figure 3. The strain gage system (Hannah et al., 1993, p. 253).

For metallic specimen it is necessary to know the general grade of metal. Especially heat-treat conditions, the alloy, modulus of elasticity, coefficient of expansion and expected property changes with test environment. Also surface condition, thickness and contour are important to know. The coefficient of expansion is necessary to know because it will dictate the type of self-temperature compensated gage required to match the test material and temperature range of test. (Hannah et al., 1993, p. 257.)

Material, surface contour, size and weight of the test part will influence the selection of the strain gage. Successful installation of strain gage depends primarily upon the bond strength achieved between the gage and the specimen. Satisfactory bond can only be achieved when the surface of the specimen is adequately cleaned. A proper cleaning procedure is necessary to determine for the particular material and specimen to be gaged. The basic cleaning procedures are mechanical, chemical and combinations of both of those. (Hannah et al., 1993, p. 257.)

The output voltage of metallic strain gages correlates with the resistance change as a function of applied strain. These resistance changes will be in the order of hundreds to a thousand

parts per million for strain levels typically encountered in experimental stress analysis. Resistance changes this magnitude are too low for indicating with ohmmeter type circuits. Therefore, it is necessary to use bridge circuit that can measure minor changes in resistance. Usually this bridge circuit is Wheatstone bridge, which is presented in figure 4. (Hannah et al., 1993, p. 12.)

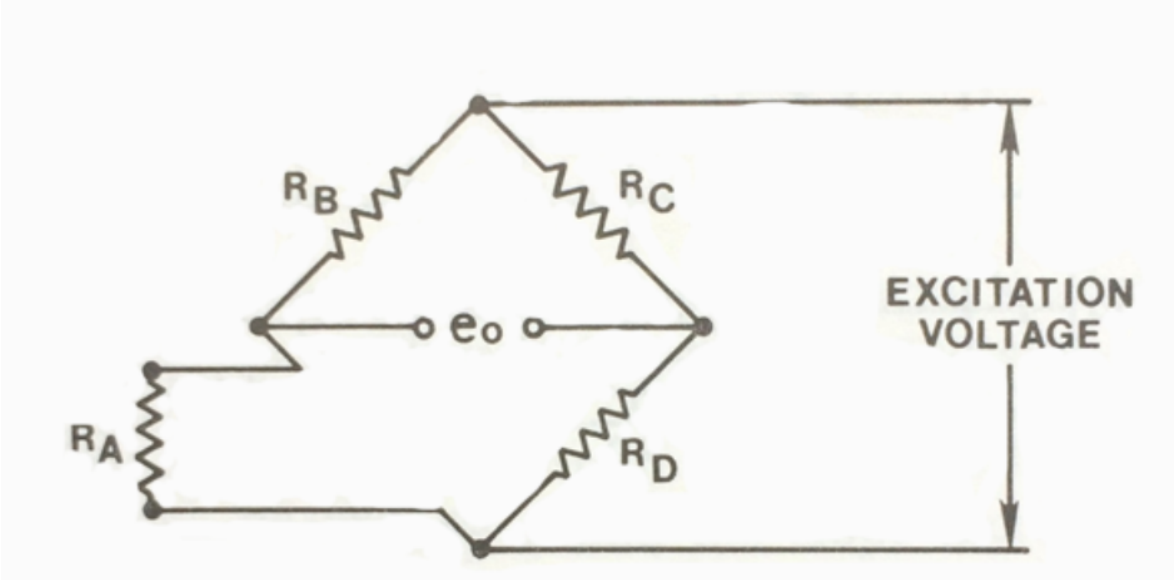

Figure 4. Basic strain gage bridge circuit (Hannah et al., 1993, p. 12).

In figure 4 R_A, R_B, R_C and R_D are resistances of strain gages and e_o is output voltage.
The basis, when calculating stresses from strains of strain gages is Hooke's law:

$$\sigma = E\varepsilon \tag{1}$$

In equation 1 σ is the stress state in the structure, E is modulus of elasticity and ε is engineering strain (Hannah et al., 1993, p. 12). Strain sensitivity is a basic bulk property of the strain-sensitive alloy, which is used in strain gage. When metal is formed into a grid, the gage will exhibit a different relationship between resistance change and applied strain. For quantifying this relationship, gage factor k is used:

$$k = (1 + 2v) + \frac{d\rho}{\rho}\frac{1}{\varepsilon} \tag{2}$$

In equation 2 $d\rho$ is resistance change in the gage in ohms, v is Poisson's ratio and ρ is resistance of unstrained gage (Hannah et al., 1993, p. 37). The bending moment can be calculated:

$$M = EW\frac{2U}{kV} = EW\varepsilon \tag{3}$$

In equation 3 W is section modulus, U is output voltage and V is input voltage. The axial force can be calculated:

$$F = AE\varepsilon \tag{4}$$

In equation 4 A is the area of the cross section (Konstruktiotekniikan mittaukset, 1993, p. 33). From equations above, the strains from strain gages can be transformed to stresses, moments and forces that affect to the trailer with different load cases.

3.5 Fatigue

Components of vehicles and machines are often subjected to repeated loads. This repeating load can lead to microscopic physical damage in materials involved. Stresses that are well below material's ultimate strength form a crack or other macroscopic damage, if cyclic loading is continued to apply. This will eventually lead to failure of the component. This whole process of damage and failure due to cyclic loading is called fatigue. (Dowling, 2007, p. 391.)

Nowadays, three approaches are used for designing and analyzing against the fatigue failures. Stress-based approach is from the year 1955. In this approach the analysis is based on nominal stresses in inspected area of the component. The nominal stress is determined by analyzing mean stresses and stress raising locations such as keyways and holes. Strain-based approach involves detailed analysis of applied location's yielding during cyclic loading at stress raiser locations. The last approach is the fracture mechanics approach, which applies growing cracks by fracture mechanics methods. (Dowling, 2007, p. 392.)

The presence of a crack can significantly reduce the strength of component due to brittle fracture. It is unusual that new component has a crack that is dangerous size, but it is still

possible if the manufacturing process is not proper. In common situation, a small flaw that was initially present develops into a crack and grows until it reaches the size when brittle fracture will occur. (Dowling, 2007, p. 392.)

Fatigue fracture forms when load is fluctuating with time and the crack at least partially closes. Fatigue fracture process can be divided in to three stages, nucleation, progression and final fracture. Generally the nucleation period takes most of the components lifetime. Progression period means that the crack grows with an accelerative rate. Progression period continues as long as the component breaks brittle or ductile. Nucleation period prolongs when ultimate strength increases. (Ikonen et al., 1991, p. 50.)

3.5.1 Effective notch stress approach

Increases in local stresses at notch that is formed by the weld root or the weld toe can be considered by using the effective notch stress approach. Effective notch stress approach is mainly used by forming fictitious notch to the structure. The idea in ENS approach is that the stress reduction in a notch can be achieved by a fictitious enlargement of the notch radius. Fictitious notch roundings are presented in figure 5. (Fricke, 2013, p. 763.)

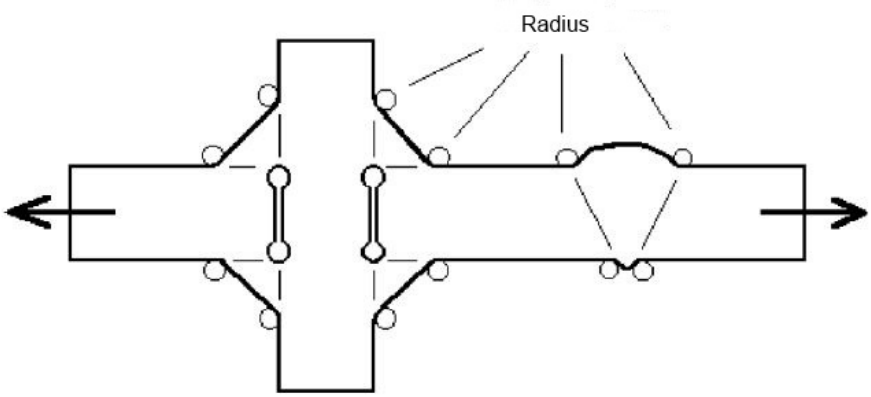

Figure 5. Fictitious notch roundings (Fricke, 2013, p. 763).

In the worst-case approach, fictitious rounding of 1 mm radius is modelled at the weld toe or root. This 1 mm radius rounding can however cause problems with structures that are thinner than 5 mm. That is because of the substantial reduction in cross section, which may

cause stress distribution distortion. That will greatly affect to the calculated fatigue life. For correct results, notch radius of 0.05 mm or even smaller is recommended to use with sheet materials thinner than 5 mm. (Fricke, 2013, p. 763.)

The major advantage of the effective notch stress approach, compared to nominal stress approach and structural stress approach is that it takes explicitly into account the local stress at the relevant notch. Weld throat thickness, actual geometry and local stress distribution are therefore taken into account. Still, the weld geometry has to be idealized. Residual stresses and other irregularities can only be considered using S-N curve. (Fricke, 2013, p. 763.)

When determining the effective notch stress by finite element analysis the element sizes has to be small enough, 1/6 of the rounding radius with linear elements and 1/4 with higher order elements. Even smaller element sizes are recommended to be used if it is possible, even the element size of 0.05 mm. These element sizes have to be used in curved parts and beginning of straight part of the notched surface in both, normal to face and tangential directions. In some applications, the element sizes in the radial direction can be the most important factor. (Hobbacher, 2008, p. 35.)

FAT classes which will be used in the ENS approach are derived from fatigue test results that are obtained from notch stress analyses and welded joints. FAT classes are presented in Table 3. These fatigue classes are derived for S-N curve slope exponent m=3 and they are based on principal stress in the notch root. If von Mises stresses are used, one category lower FAT class should be applied. (Fricke, 2013, p. 764-765.)

Table 3. Characteristic FAT classes for steel based on maximum principal stress (Fricke, 2013, p. 765).

Material	Characteristic fatigue strength for notch reference radius = 1 mm	Characteristic fatigue strength for notch reference radius = 0.05 mm
Steel	FAT 225	FAT 630

From the finite element analysis results and the determined equivalent stresses at the notch, the fatigue life for welded joints can be calculated. In this work FAT-class 630 is used, because of the thin profiles. Cycles to failure can be calculated:

$$N = \left(\frac{FAT}{\Delta\sigma_{eff,eqv}}\right)^{m} \cdot 2 \cdot 10^{6} \quad (5)$$

In equation 5 N is cycles to failure, $\Delta\sigma_{eff,eqv}$ is equivalent notch stress and m is slope exponent of S-N curve. (Niemi, 1993, pp. 243.)

3.5.2 Structural hot spot stress approach

The hot spot stress includes all structural detail's stress raising effects. Non-linear peak stresses that are caused by local notches for example weld toes are excluded from the structural stress. These non-linear peaks are noticed in the method by FAT-class. Structural hot spot stresses can be defined for shell, tubular structures and plate. (Hobbacher, 2008, p. 24-31.)

Typically, the hot spot stress approach is used when the geometry is complicated and no clearly defined nominal stress can be determined. The structural stress is determined by using reference points that will help to extrapolate the stress at the weld toe. In figure 6 is presented how the structural hot spot stress is defined. (Hobbacher, 2008, p. 24-31.)

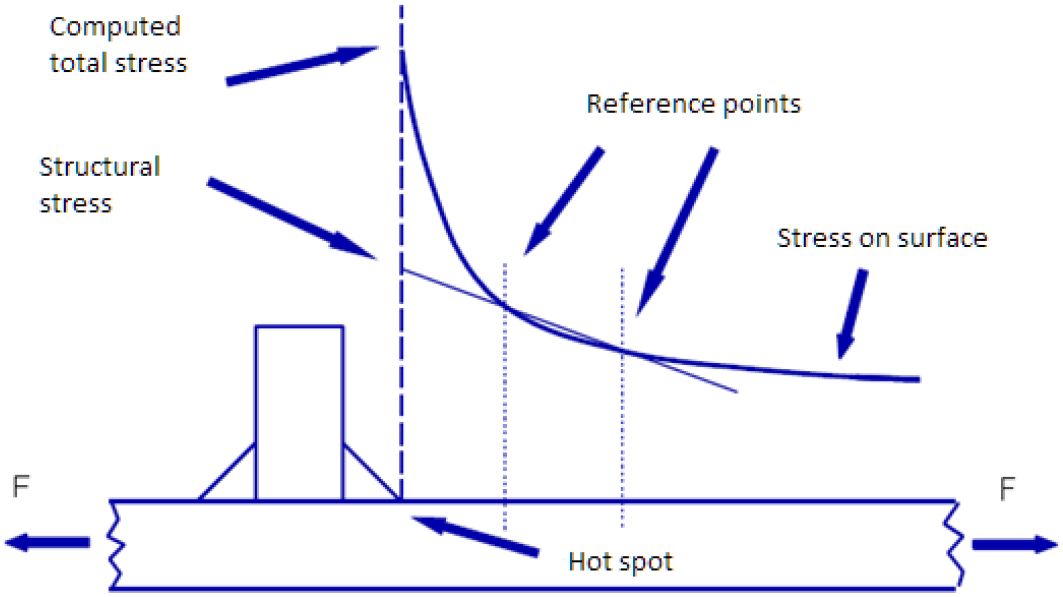

Figure 6. Hot spot stress definition (Hobbacher, 2008, p. 24-31).

The hot spot stress is determined from idealized weld joints with FEA. Any misalignments of welds have to be taken into account by stress intensity factor or by modelling the misalignment to FEA model. When the hot spot stress is determined by extrapolation, the element lengths has to be determined by the reference points selected for stress evaluation. The closest stress near the hot spot is measured from the first nodal point. This means that the element length is equal to the distance of the first reference point. With finer meshes, the number of elements through the plate thickness has to be considered also. Proper element widths are important especially when the stress gradient is steep. The width of solid element should not exceed the attachment width in front of the attachment. (Figure 7.) (Hobbacher, 2008, p. 24-31.)

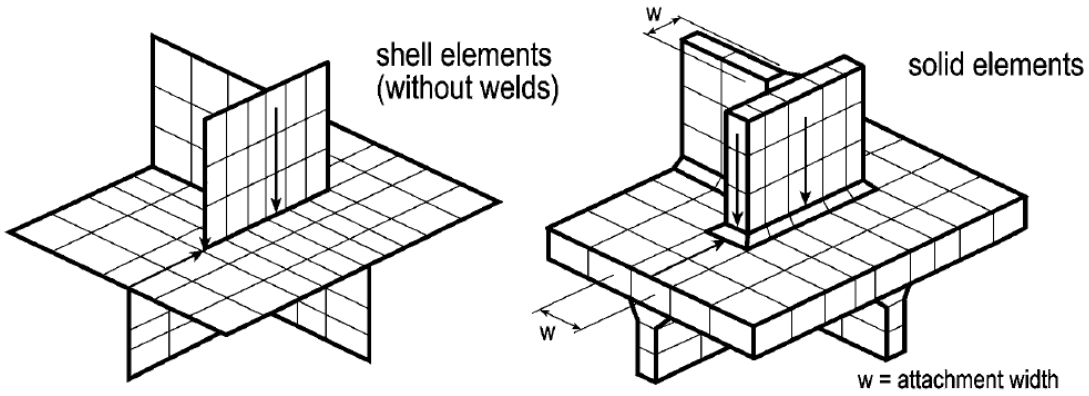

Figure 7. Typical meshing for hot spot approach (Hobbacher, 2008, p. 24-31).

When the hot spot stress increases linearly towards the weld toe, the distances of the reference points in which the nodal stresses are determined are 0.4·t and 1.0·t. Type a structural hot spot stresses are determined by using reference points and extrapolation equation presented in equation 6. (Hobbacher, 2008, p. 24-31.)

$$\sigma_{hs} = 1{,}67 \cdot \sigma_{0{,}4 \cdot t} - 0{,}67 \cdot \sigma_{1{,}0 \cdot t} \quad (6)$$

In equation 6 σ_{hs} is structural hot spot stress, $\sigma_{0,4t}$ and $\sigma_{1,0t}$ are stresses at distances of 0.4·t and 1.0·t. In Table 4 is presented the recommended meshing and extrapolation for the hot spot approach. These are used when modelling hot spot stress finite element model.

Table 4. The recommended extrapolation and meshing for hot spot approach. (Hobbacher, 2008, p. 24-31).

Type of model and weld toe		Relatively coase models		Relatively fine models	
		Type a	Type b	Type a	Type b
Element size	Shells	t x t max t x w/2*)	10 x 10 mm	≤0.4 t x t or ≤0.4 t x w/2	≤ 4 x 4 mm
	Solids	t x t max t x w	10 x 10 mm	≤0.4 t x t or ≤0.4 t x w/2	≤ 4 x 4 mm
Extra-polation points	Shells	0.5 t and 1.5 t mid-side points**)	5 and 15 mm mid-side points	0.4 t and 1.0 t nodal points	4, 8 and 12 mm nodal points
	Solids	0.5 and 1.5 t surface center	5 and 15 mm surface center	0.4 t and 1.0 t nodal points	4, 8 and 12 mm nodal points
*) w = longitudinal attachment thickness + 2 weld leg lengths **) surface center at transverse welds, if the weld below the plate is not modelled (see left part of fig. 2.2-11)					

When calculating the fatigue life for the structure by using hot spot stresses, prepared S-N curves are used. Now the FAT class is based on the fluctuation of hot spot stress so they are included by the geometrical influences. Two types of hot spot FAT classes can be used. These classes are 90 and 100. In Table 5 is presented some FAT-classes for different kind of structural details. The fatigue life with hot spot stress approach can be calculated:

$$N = \left(\frac{FAT}{\Delta\sigma_{hs,eqv}}\right)^m \cdot 2 \cdot 10^6 \tag{7}$$

In equation 7 $\Delta\sigma_{hs,eqv}$ is equivalent structural hot spot stress. (Hobbacher, 2008, p. 24-31)

Table 5. FAT classes for hot spot stresses (Hobbacher, 2008, p. 24-31).

No.	Structural detail	Description	Requirements	FAT Steel	FAT Alu.
1	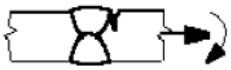	Butt joint	As welded, NDT	100	40
2	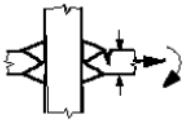	Cruciform or T-joint with full penetration K-butt welds	K-butt welds, no lamellar tearing	100	40
3	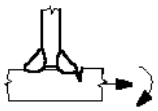	Non load-carrying fillet welds	Transverse non-load carrying attachment, not thicker than main plate, as welded	100	40
4	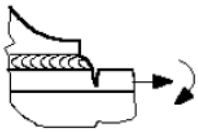	Bracket ends, ends of longitudinal stiffeners	Fillet welds welded around or not, as welded	100	40
5		Cover plate ends and similar joints	As welded	100	40

4 STRAIN GAGE MEASUREMENT

The main target of strain gage measurements is to determine the correct stress state of structure. The measurement plan is made with FEA to determine the locations where the greatest stresses are located and with strain gage measurements the real stress state is then determined.

4.1 Measurement plan

A simple shell element medial surface FE-model was made for the measurement plan from the boat trailer geometry. In this pre-analysis the loading was set according to report that was made by Majava Group. Based on this medial surface model and its stresses, the locations of strain gages were determined. The strain gages were set to places, where the greatest stresses located in the trailer. Two of the strain gages were set to measure the bending moment and axial forces at the shaft. This was because from the results of these strain gages, total applied force at trailer hitch could then be determined and the correct loading set for the FEA. The measurement plan is presented in Appendix I.

The most critical locations of the structure according to measurement plan will be the two joints of the shaft and transverse beams. These locations are under the main investigation. Test drive rounds will be performed for four different load cases and obstacle overrun will be done after each round. Depending on the conditions, the loading of the trailer with boat is performed before each test drive round. If it seems to be too complicated, this stage will be improvised later from snow bank if possible.

4.2 Measurement process

Unisigma carried out the strain gage measurements. Unisigma did the installation and calibration of strain gages and also recorded each measurement step on computer and handled the post-processing of the data after the measurements were completed.

When the trailer was seen in reality it was noticed that the geometry of the trailer had changed a little compared to the one, which the measurement plan was made from. In this new geometry there was no lug for the suspension and the supporting of the wheels and axle

was different. That meant that hot spot measurement from the lug could not be done. Some changes were also made for the rest of the strain gage locations. The final locations of strain gages are presented in figures 8-12.

The strain gage measurement process consisted three main steps. Those steps were static measurements, test drives in public roads and finally lifting and dropping the boat from the trailer. Different load cases were applied on trailer and boat combination during these steps. The maximum load that is allowed for the combination is 750 kg. It includes the mass of the trailer, which is 178 kg. Six strain gages were installed into the trailer's frame. The locations of these strain gages are presented in figure 8.

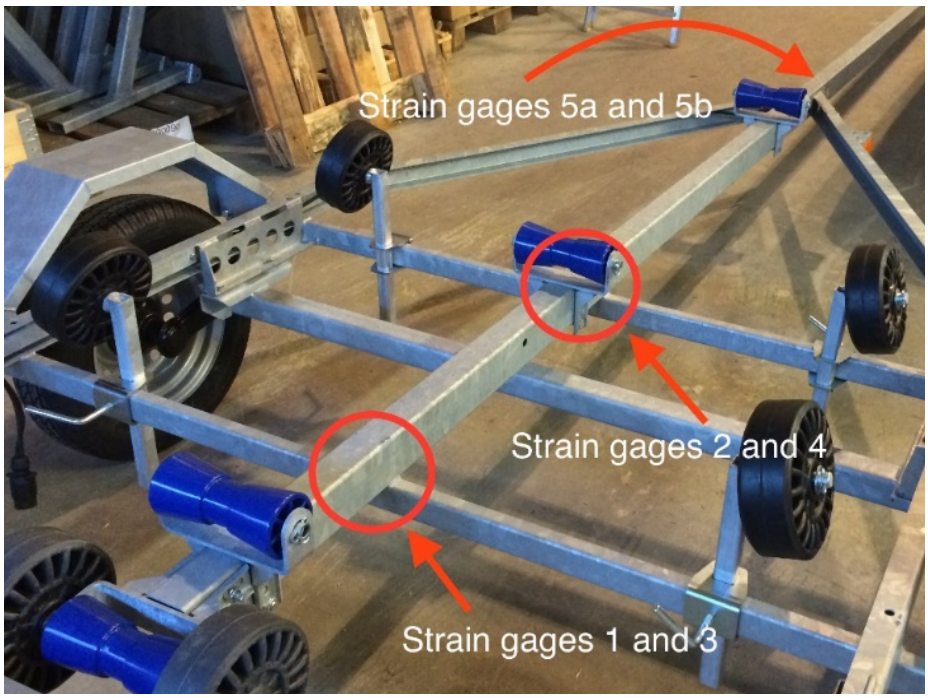

Figure 8. The locations of strain gages.

The strain gage 1 (SG1) was installed into the rear transverse beam at 2.6 mm distance from the weld toe and the strain gage 3 (SG3) was installed under the shaft at 3.1 mm distance from weld toe. (Figure 9.)

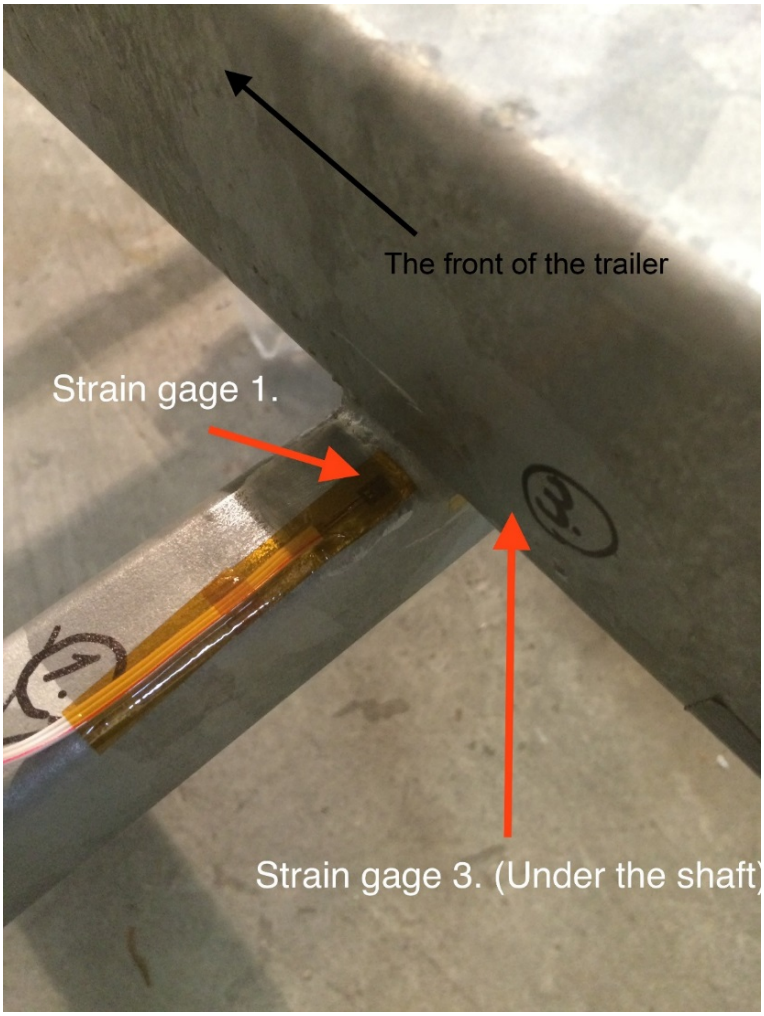

Figure 9. Strain gages 1 and 3 at the rear weld joint.

The strain gage 2 (SG2) was installed on the front transverse beam at 2.4 mm distance from weld toe and the strain gage 4 (SG4) under the shaft at 2.0 mm distance from weld toe. (Figure 10.)

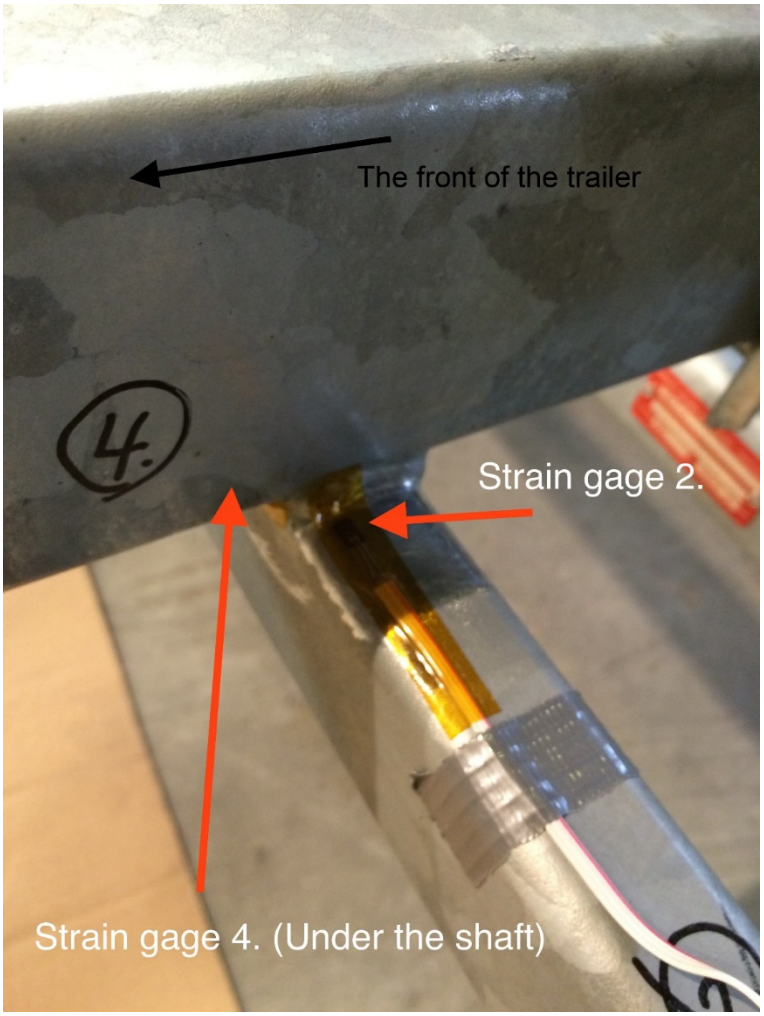

Figure 10. Strain gages 2 and 4 at the front weld joint.

Strain gages 5a (SG5a) and 5b (SG5b) were installed at the distance of 2.14 m from the trailer hitch. These strain gages measured the bending moment and axial force from the shaft. (Figure 11.)

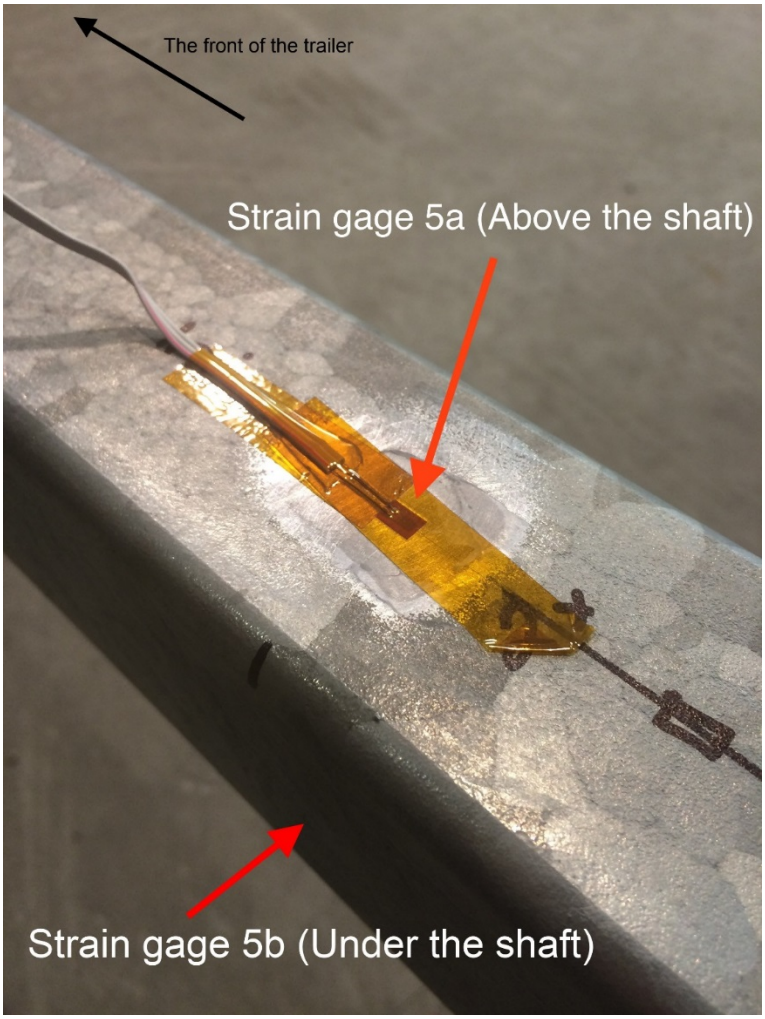

Figure 11. Strain gages 5a and 5b in the shaft.

The desirable condition 0.4·t distance from the weld toe was not fulfilled for any of the strain gages 1-4, because of practical reasons. The results from these strain gages are used to find out the most critical location of the structure and to determine correct loading for later finite element analyses. The achieved strain gage distances from the weld toe are presented collectively in Table 6.

Table 6. Strain gage distances from weld toe.

	SG1	SG2	SG3	SG4
Distance from weld toe [mm]	2.6	2.4	3.1	2.0

After the installation was completed, the output voltage of the Wheatstone bridge was set to zero, so the zero level is in situation, where the trailer lies on its own weight.

In figure 12 is presented the weights that were used to load the boat for different load cases. The mass of single heavier weight was 15.5 kg and the mass of single lighter weight was 5.5 kg. The heavier weights were used to determine the correct engine load at the rear of the boat so only the lighter weights were moved when changing between the load cases. In Table 7 is presented the masses that will lead approximately to total weight of 750 kg.

Figure 12. An example of weight distribution. Rear-heavy load case.

Table 7. Masses of parts.

Part	**Weight [Kg]**	**Quantity [Pc.]**	**Total weight [Kg]**
Boat	273	1	273
Trailer	178	1	178
Light extra weight	5.5	38	209
Heavy extra weight	15.5	6	93
∑			753

When everything was tested and proved to be working properly, static measurements began. Static measurements consisted seven stages. After static measurements were completed, test drive started. The test drive implementation order was changed compared to the one that was planned in measurement plan because of practical reasons. One test drive round lasted approximately 45 minutes and was 43.5 km long in total. The tarmac road driving included 80 km/h and 50 km/h roads and the total length driven on tarmac was 23.5 km. The gravel road driving included 50 km/h roads and the total length driven on the gravel was 20 km. The test drive round was the same for all four load cases. The load cases and measurement stages are presented in Appendix II.

At the beginning it was planned to make the test drive round also with overload, but after the test drive roads were chosen, this plan was abandoned. That was because of the public roads and the trailer regulations. Only static measurements were performed with overload. There were two different overload cases and those were determined according to the weights that were available. At its best, the total weight of the trailer and boat combination was approximately 1170 kg, which is 420 kg over the allowed.

Before the first test round, the driver was told to drive as he would in normal life, so the results would be as close to reality as possible. When the first test round was completed, some notices were made about the weather conditions. Because of the wintertime, the gravel roads were slightly smoother than in summer time. That was because of the snow that had smoothed the bumps of the gravel roads. In summer time these bumps could be tougher to the trailer. It is hard to say the true difference between the effects of gravel roads between winter and summer time. The tarmac coating was dry and there were no snow or ice on it, so the results correspond with summertime conditions. After each test drive, an obstacle

overrun was performed with wood plank for two different overrun cases. Those cases were overrun with left tire and overrun with both of the tires. All of the overruns were performed with speed of 20 km/h.

When the test drive rounds were performed, the loading of the trailer with boat stage could begin. The boat was lying on snow bank, where it was first lifted on trailer and then dropped back off. Because of the wintertime, there were no ice-free lakes so the process had to be improvised. The boat was dropped on snow bank, where it could be lifted back on the trailer (Figure 13.). This process turned out to be hard to accomplish because there were no help from the water that normally supports the boat while the trailer is reversed partially under it. The boat was also very heavy, because it was loaded up to top allowed weight. Decisions were made and only two lifts and drops of the boat were accomplished, one with front-heavy load and one with rear-heavy load.

Figure 13. The snow bank in which the boat was dropped.

4.3 Measurement results

The measurement data was firstly processed by Unisigma. The result data included static strains for each load case, time history graphs, rainflow accumulations from test drives and notes that were made from each measurement stage. In figure 14 is presented an example of time history graph that was obtained from one of the strain gages after test drive round.

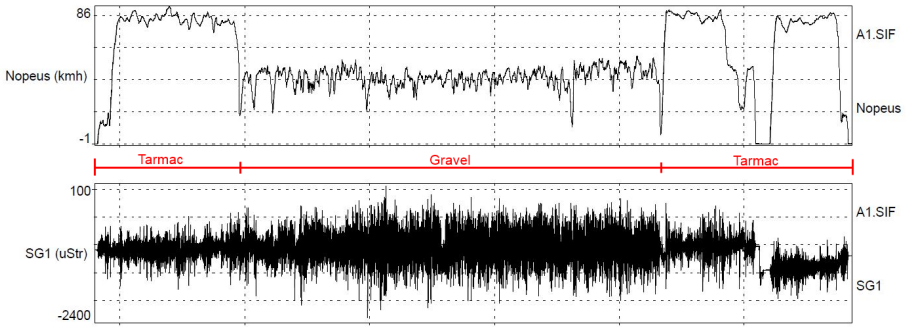

Figure 14. An example of time history graph.

The results of static measurements are presented in Appendix III. Static results are used to determine the correct loading for FE-analyses and also for analytical calculations. From the results of strain gages 5a and 5b, the correct reaction forces at the trailer hitch can be calculated for each load case. In fatigue calculations the entire measurement data from test drive run is used with each load case. This is because of the need of as realistic results as possible. The loading of the boat on trailer data is measured separately and it is added to test run data afterwards. This kind of procedure takes into account the whole trailer usage.

For fatigue calculations, equivalent stresses are calculated by using the stress history data from test drives. In Appendix III is presented the equivalent stresses for the different load cases on tarmac and gravel roads. For the strain gages 5a and 5b, the combined bending stresses are presented. Equivalent stresses are calculated:

$$\Delta\sigma_{eqv} = \sqrt[3]{\frac{\sum n \cdot \Delta\sigma^m}{N_{ref}}} \tag{8}$$

In equation 8 $\Delta\sigma_{eqv}$ is the equivalent stress calculated from stress history, n is the amount of stress ranges $\Delta\sigma$ and N_{ref} is the amount of load cycles. (Niemi, 1993, p. 243.)

According to the results of the strain gage measurements, the most critical location of the structure is the rear weld joint. It is the location from where the closer examinations are made from. (Figure 15.)

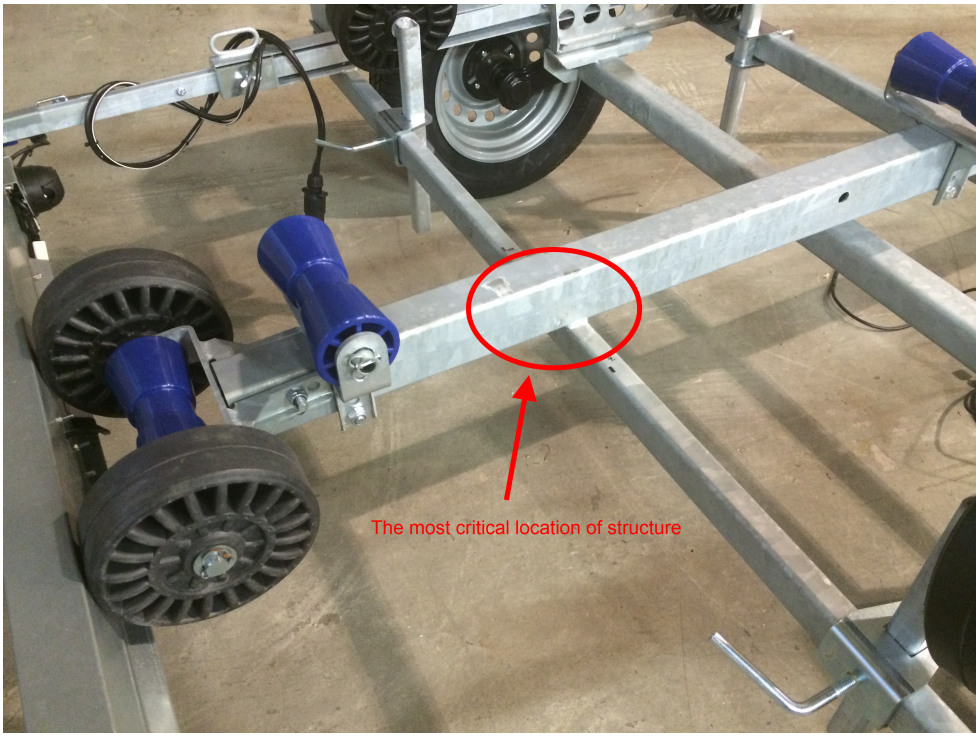

Figure 15. The most critical location of the structure.

4.4 Discussion of the measurement results

Only one test drive round was completed with each load case. Luckily the rounds could be performed without any significant impediments. There was not much traffic and the driving speeds that were planned to use in every particular section of the route could be used.

The result data from measurements is presented in Appendix III. First impressions from the static measurement data is that the strain gages that should have had tension, had tension in them and the ones that should have had compression in them, had compression. This means that the measurement plan that was made from the original trailer was successful. The little difference in the trailer geometry and the loading that was used in the measurement plan did not affect too much to the stress distribution with this trailer from which the measurements were taken at the end. Despite the geometry that was slightly different than firstly expressed. After all, the meanings of the measurement plan and later the FEA was to find out the most critical locations of the structure and to predict the correct locations for the strain gages.

When comparing the shaft's bending data from strain gages 5a and 5b between all of the load cases, there is a lot of variation in the results. This means that different load cases which

were applied to the structure had enough variation between them. These different load cases were carried out by moving 209 kg of weight at the different locations of the boat. The difference between load cases was tried to make as great as possible. There were totally 38 weights that were moved between different load cases so the weights had to be fastened with care. These weights had to stay in the boat when driving on bumpy gravel roads. The large number of weights limited little bit the wanted weight distribution, because now the loading could not be set as spot load as wanted. This was a little problem especially in the front of the boat where there was already little space because of the shape of the boat.

It was also planned to measure shear stresses from the transverse beams both sides of the shaft. This idea was later abandoned because of the financial reasons and time management. With static front-heavy loading, the stresses in strain gages 1 and 2 are the smallest when comparing to the other load cases and the stresses in same strain gages. That dictates that the shaft will take the most of the loading and the transverse beams will be less loaded. When inspecting the data from the strain gage 4, which is located under the shaft, near the front transverse beam, the stresses are clearly largest with front-heavy loading.

The test drive data and calculated equivalent stresses for fatigue calculations in Appendix III are specified for tarmac and gravel road data. From strain gages 5a and 5b, only the combined bending data is presented in the results. This is because the axial stresses were so small that the effects to the trailer's durability would not be great. Axial stresses depend largely how the car and trailer combination is driven. Sudden and hard braking causes larger axial stresses to the shaft than if the braking is made with care. The acceleration cause also some axial stresses to the shaft, but in both cases the tire slipping set the limits. The different weight distributions can cause some differences in axial stresses when braking and accelerating. When driving with even speed, the axial stresses are overall minor except the stress peaks from the roughness of the road. Test drive rounds were performed without any significant traffic and with no hurry, so the combination could be slowed down carefully when approaching crossroads so the axial stresses formed small. In analytical calculations in Appendix IV only the bending data is noticed.

Overall the equivalent stresses in the gravel data are a lot larger than in the tarmac data. Gravel road's fatigue effect to structure is therefore much greater. The total driven distances

on tarmac and gravel roads were approximately 20 km on both pavements. In reality the trailer is probably driven on tarmac most of its service life. This factor is taken into account when calculating the total service lives for the trailer with different load cases. Test drive had to be completed with long enough routes to get as realistic results as possible. The longer the route is, more reliable the results are. The ideal situation would have been to drive a few test drive rounds with each load case, but now it was not possible because of the limited time.

When comparing the test drive data and equivalent stresses between the strain gages of a single load case, with flat load case and the empty trailer case the strain gage 1 has the greatest equivalent stresses with both of the load cases. The strain gage 1 is located near the rear transverse beam's weld joint. This happens with both gravel and tarmac data and means that the worst location in fatigue perspective is the rear weld joint. The strain gage 3 has the smallest equivalent stresses in it with these load cases.

With rear-heavy and front-heavy loading the greatest equivalent stresses form to the strain gage 2 near the front transverse beam's weld toe. This is something that was not expected from the static analyses. After all, the greatest equivalent stress values of all load cases in both of the strain gages 1 and 2 form with the flat load case, so it is the most critical load case for the structure in fatigue perspective and it is the load case for which the fatigue analysis with FEA will be performed.

The loading of the trailer affects to the trailer's fatigue life and loading the trailer differently can increase its durability. For example, setting the winch of the trailer closer to the trailer hitch will move boat's center of the gravity forward. This will decrease the stresses in the rear transverse beams weld joint, which seems to be the most critical location of the trailer.

When comparing the test drive bending data from strain gages 5a and 5b there is also much difference between the results of load cases on gravel and tarmac. On tarmac the greatest equivalent bending stresses form with rear-heavy load case. On gravel the flat load case forms the greatest bending stress to the shaft. Front-heavy loading, which had the greatest stresses in the shaft in static measurements, has now the lowest equivalent bending stress. This dictates that the front-heavy loading makes the trailer and boat combination more stable

and the stress variations will be smaller. This forms smaller the equivalent stresses, which are critical for the fatigue.

The empty trailer seems to have higher equivalent stress values in strain gages 3 and 4 than front-heavy and flat load cases. It seems to be that the trailer is not so stable when driving empty and the suspension has its own affect it also. These strain gages 3 and 4 were installed under the shaft, so they measure the stresses that form from the bending of the shaft. When a boat is tied up on the trailer, the combination becomes stiffer and the equivalent stresses in these locations form smaller. The vibrations in the shaft will become smaller.

Loading and unloading the trailer with boat had to be improvised because of the winter conditions. The boat was dropped on snow bank, where it was then lifted back up on the trailer. This kind of procedure causes higher stresses to the trailer than normal lifting will cause, when it is performed from water. The greatest stress in strain gage 1 in this lifting process was with rear-heavy weight load case. It was approximately 450 MPa, which is over the yield strength of the material. It will be even greater at the weld toe, because the strain gage was installed at the distance of 2.6 mm from the weld toe. This stress is after all only temporary and short term so the trailer can be assumed to last this kind of extreme lifting process, which will be rare for the trailer in real use. Normal situation where the trailer rests on water will be much easier for the trailer and the rear weld joint to receive.

5 FINITE ELEMENT ANALYSIS

Finite element analysis is performed with Femap and Abaqus softwares. A simple medial surface model was created for the measurement plan with Femap. Closer examinations are performed with solid element models, which are modeled and analyzed with Abaqus.

Closer analyses are performed to load cases, which form the greatest stresses to structure according to strain gage measurements. For static analyses the most critical load case is the rear-heavy weight load case. For fatigue the most critical case is the flat load case. Fatigue analysis is also made for empty trailer, because the normal use of the trailer consists also driving with empty trailer. According to the measurement results, stresses in empty trailer driving are also significant. The fatigue calculations are made with effective notch stress and hot spot stress approaches. At the end comparison is made between the results of these approaches.

One of the main goals of FEA is to determine if it is reasonable to change the trailer's material to high strength steel. S420 material trailer's shaft's profile is 80x60x3 and transverse beam's 50x30x3. Weight reduction is tried to achieve in the trailer's frame, so the profiles used with option material Form 800 is now 80x60x2 in the shaft and 50x30x2 in the transverse beams. Only the profile thickness is therefore changed with this Form 800 material.

Firstly a sparse mesh was applied to structure to determine the equivalent loadings for the FEA-models that correspond to the strain gage measurement results. For more accurate results, a submodel was modeled from the locations, where the greatest stresses located in the structure. Loadings for models are set to the centers of gravity of the boat. The centers of gravity are firstly determined from the strain gage measurement results and then corrected by comparing the measurement data from every strain gage and FEA to achieve a correlation factor 1. The center of gravity is then connected to the model by using coupling elements on surfaces of the shaft. The supporting of tires is simplified and suspension is not taken into account in these analyses. Tire supporting points are set to locations where the tires are located in real structure and they are then connected to the trailer′s frame with steel rods. The entire trailer is used in analyzing, because the number of elements was not very large and

therefore the analyzing times were short. The closer examinations from the locations where the greatest stresses stand are made after all with more exact mesh and with submodels. (Figure 16.)

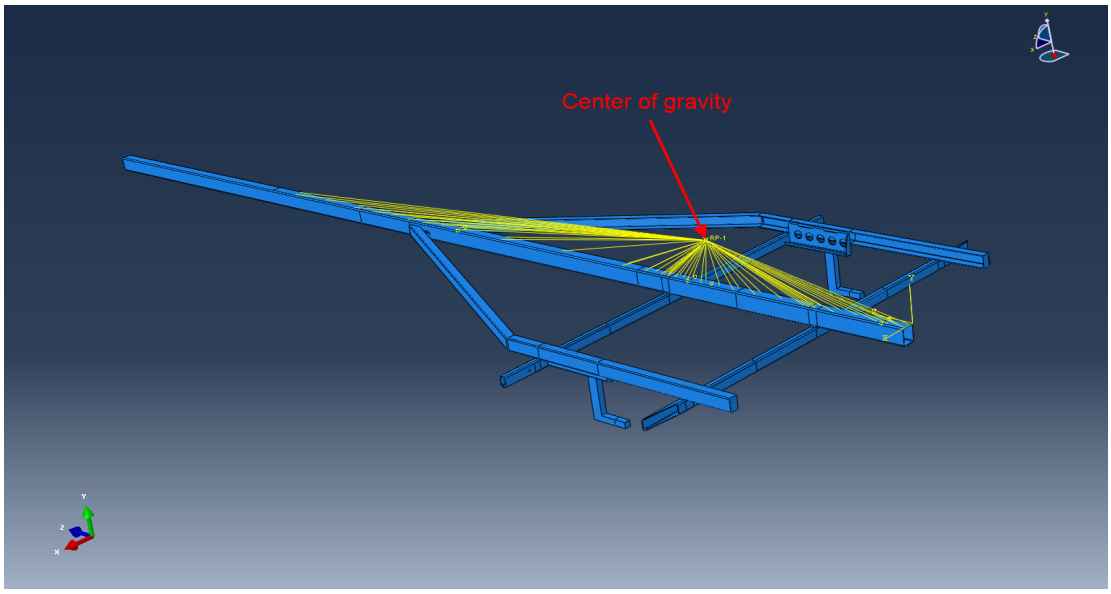

Figure 16. An example of load setting to the center of gravity.

The meshing of the entire trailer model is done with tetrahedral solid elements. Finer mesh is applied to the rear part of the trailer, because of the need for better result accuracy. (Figure 17.)

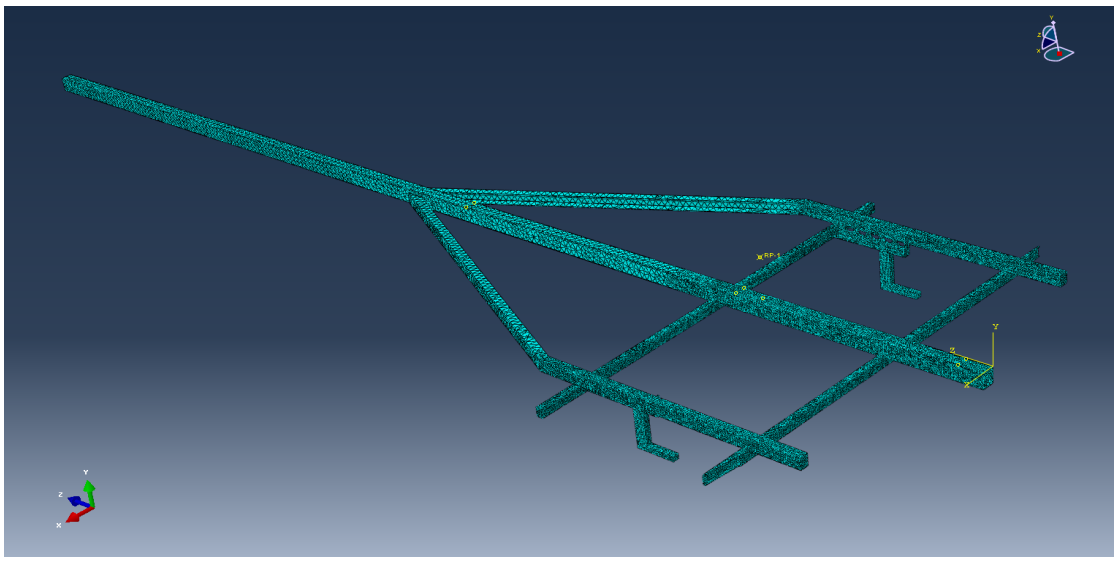

Figure 17. An example of meshing of the whole trailer structure with tetrahedral solid elements.

The constraints of the entire model are set according to situation, where the trailer is attached to trailer hitch. Only rotations are allowed at the trailer hitch. At the tire mounting points the translations to X and Y directions are forbidden. The behavior and total deformation of entire model are presented in figure 18.

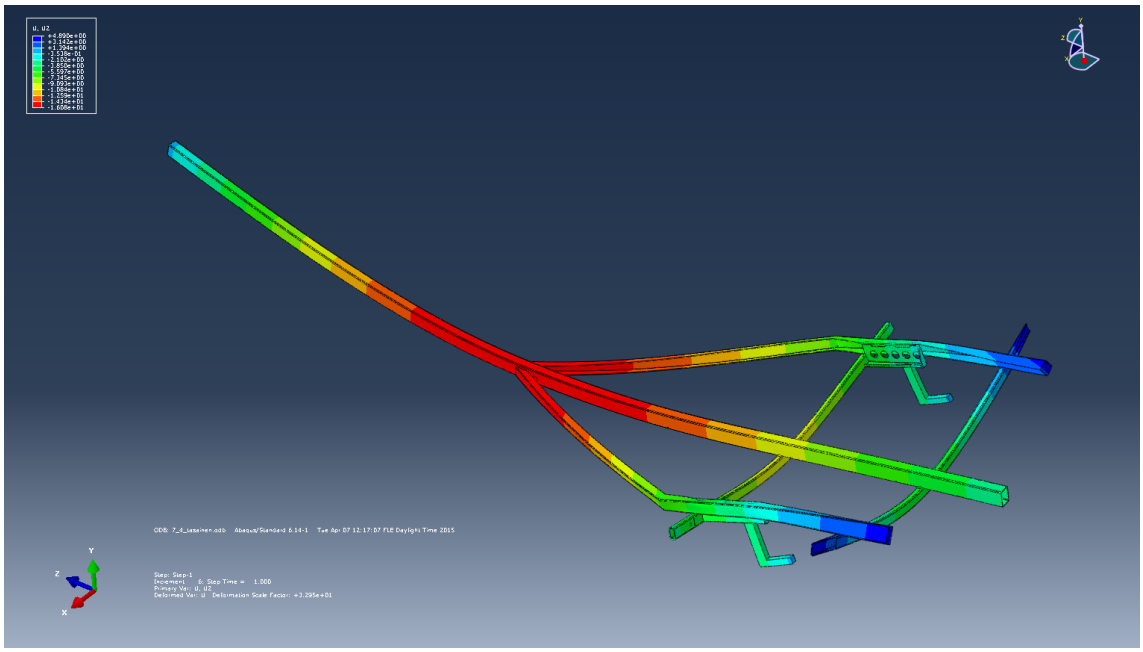

Figure 18. An example of behavior of the model with flat load case.

5.1 Results from FEA

The results are presented for current material S420 structural steel and the option material high strength rectangular precision tube Form 800. Static results and fatigue life results from ENS and hot spot approaches are presented for both of the materials.

5.1.1 Analyses with S420

The most critical location of the structure is the rear weld joint of shaft and transverse beam with all load cases. An example of performed static analysis is presented in figure 19 with rear-heavy load case and von Mises stresses.

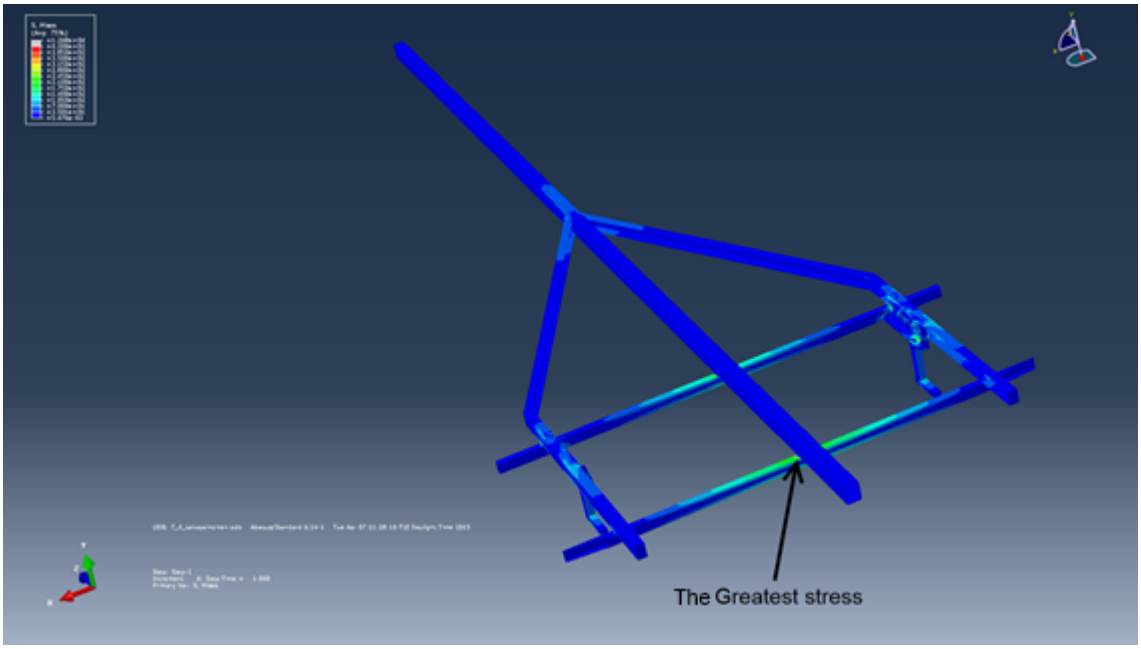

Figure 19. The stress distribution of the trailer structure with rear-heavy weight load case. Stresses are limited to 420 MPa von Mises stresses.

Closer static examinations for rear weld joint are made with submodel. It is presented in figure 20 for rear heavy load case. Submodel is meshed with finer mesh than the entire model and with tetrahedral solid elements.

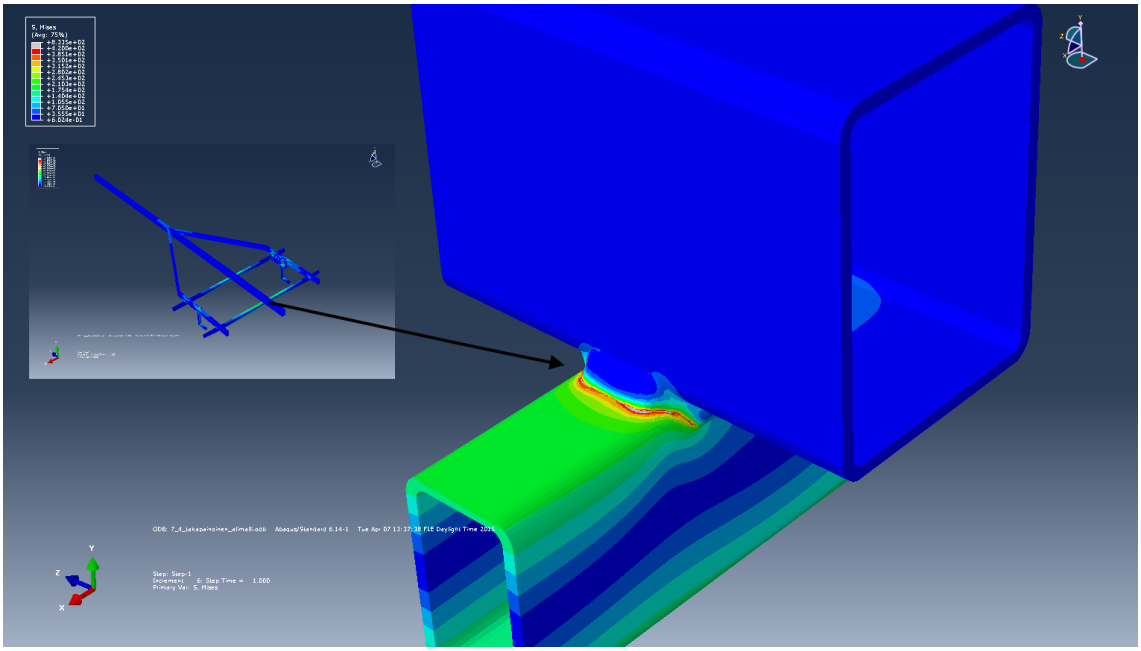

Figure 20. Static rear-heavy weight load case. Rear weld joint stresses. Stresses are limited to 420 MPa von Mises stresses.

Static analysis is made also with the greatest overload case. The loading was set according to the data from Appendix III. The results of this greatest overload case are presented in figure 21 and Table 8.

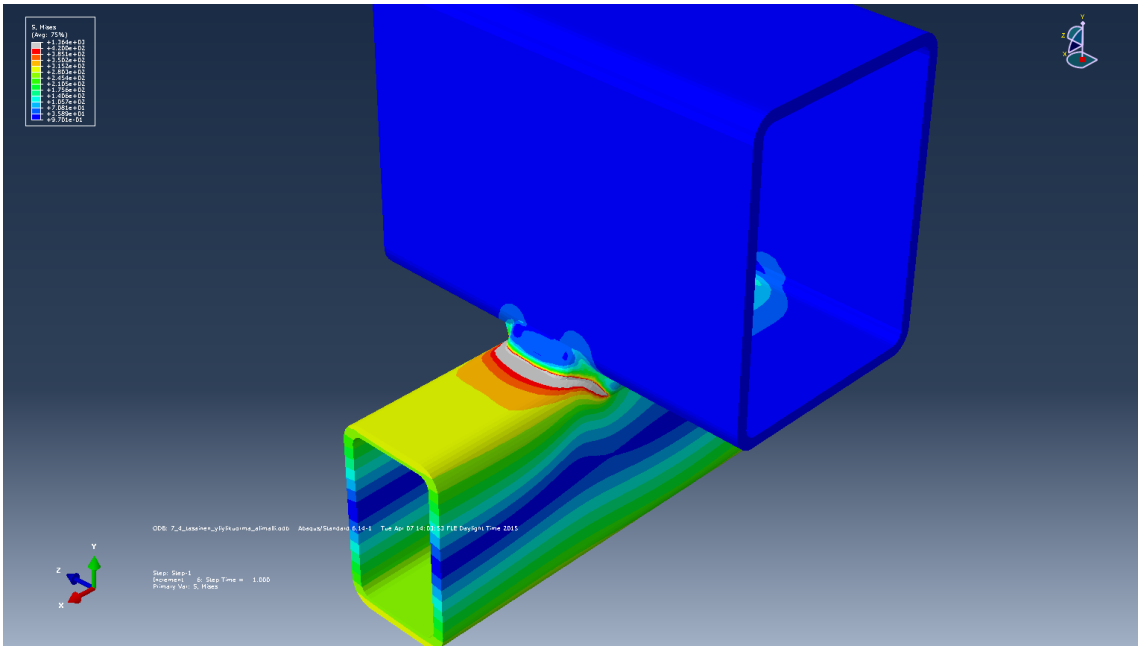

Figure 21. Static greatest overload case. Rear weld joint stresses. Stresses limited to 420 MPa von Mises stresses.

Table 8. Static analysis results with S420 structural steel. The greatest stresses at the rear weld joint's weld toe.

Load case	**Stress at the weld toe [MPa]**
Flat load	440
Front-heavy load	410
Rear-heavy load	490
Greatest overload	780

Total deformations with S420 material are presented in Table 9. The greatest deformations form to the center of the shaft. It is the location where U-profiles attach to it.

Table 9. Total deformations with S420 structural steel.

Load case	**Total deformation [mm]**
Flat load	16,1
Front-heavy load	23,1
Rear-heavy load	11,4
Greatest overload	27,8

Fatigue analyses are performed for flat load and empty trailer load cases. The flat load case had the greatest equivalent stress of all cases in the most critical location of the structure. The empty trailer case need to be investigated when analyzing the trailer's total fatigue life, because it is assumed that the trailer's service life consists large amount of empty trailer driving. Results are presented from ENS and hot spot approaches.

The thicknesses of the profiles are 3 mm for S420 and 2 mm for Form 800 so for fatigue analyses with ENS approach 0.05 mm radius roundings are modeled at the weld roots and toes. Now the element size near the weld toe has to be 0.008 mm or smaller (Hobbacher, 2008, p. 35). Because of this very exact meshing, the submodel had to be modeled from very small area. Otherwise the number of the elements would become too large and the analyzing times too long. In figure 22 is presented the stress distribution from the ENS approach at the weld root and toe, where it can be seen that the weld toe has much greater stresses than the weld root. According to this information the more accurate submodel is made from the weld toe, at the location where the stress is the greatest.

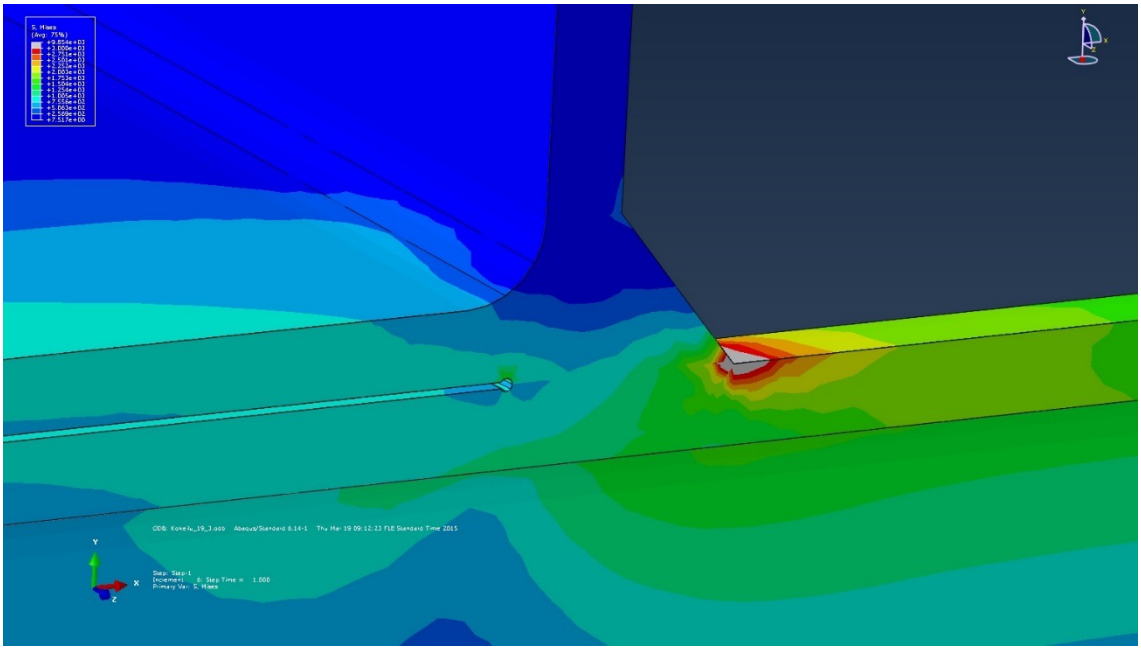

Figure 22. An example of stress distribution at the weld root and toe with ENS approach.

In figure 23 is presented the location where the submodel is made from. It is located at the rear weld joint's rear corner. The submodel is modelled from very small area because of the need of very exact meshing.

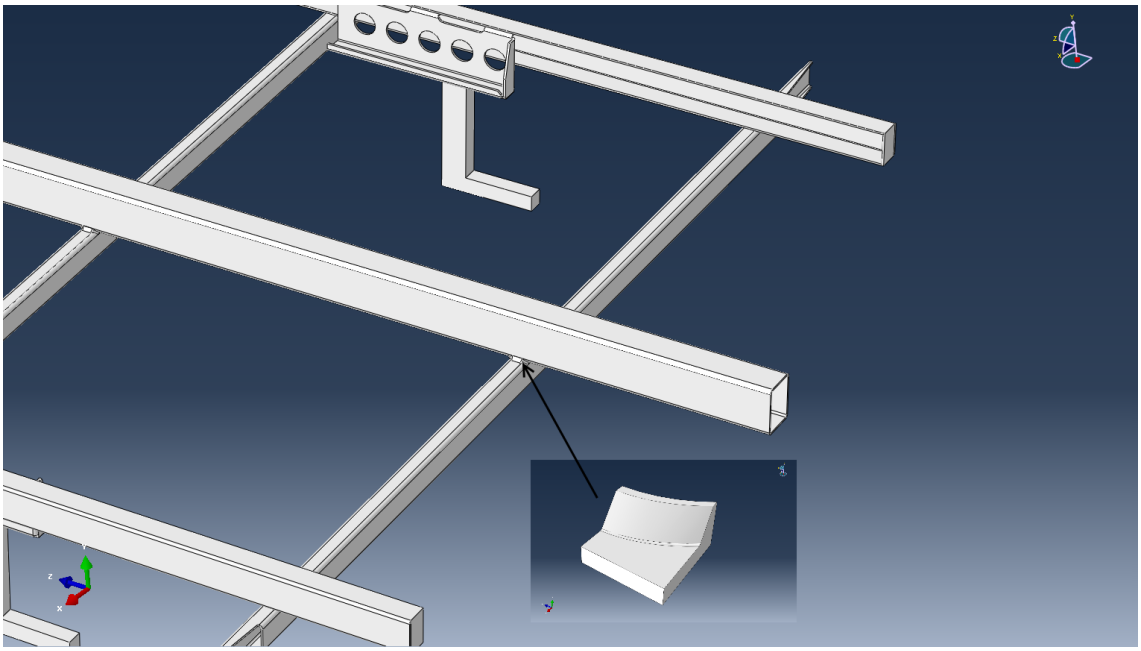

Figure 23. A submodel from the rear weld joint for fatigue calculation.

The meshing of the submodel is presented in figure 24. At the rounding that are modeled at the weld toe the mesh is finer than elsewhere in the submodel. All the elements used in this submodel are hexahedral solid elements.

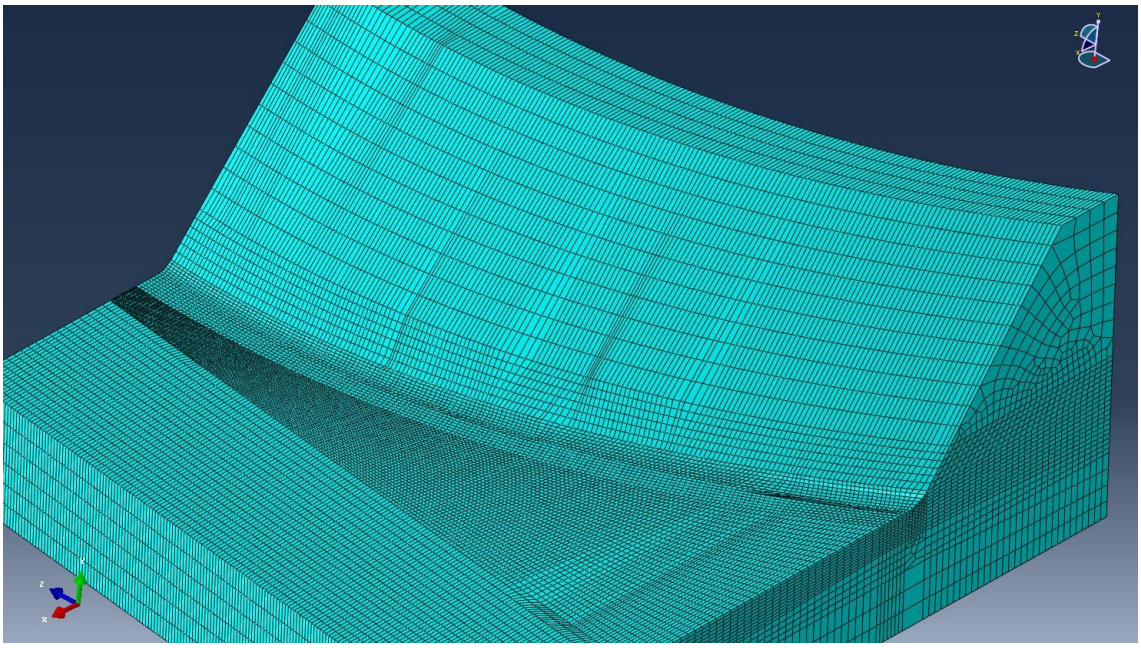

Figure 24. Meshing of submodel of rear weld toe.

In figure 25 is presented the ENS approach results of flat load case analysis on tarmac. This kind of submodel analysis is made to four cases and the results are shown in Table 10. The stresses in figure 25 are maximum principal stresses. In Table 10 is also presented the calculated fatigue lives for the trailer's rear weld joint in kilometers with ENS approach. The flat load case has the greatest equivalent stresses, it is also the most critical for fatigue. In calculations also the empty trailer usage is noticed, because it is assumed that the normal usage includes also empty trailer driving. The lengths of test drive routes were on tarmac 23.5 km and on gravel 20 km. Fatigue calculation example is shown in Appendix V.

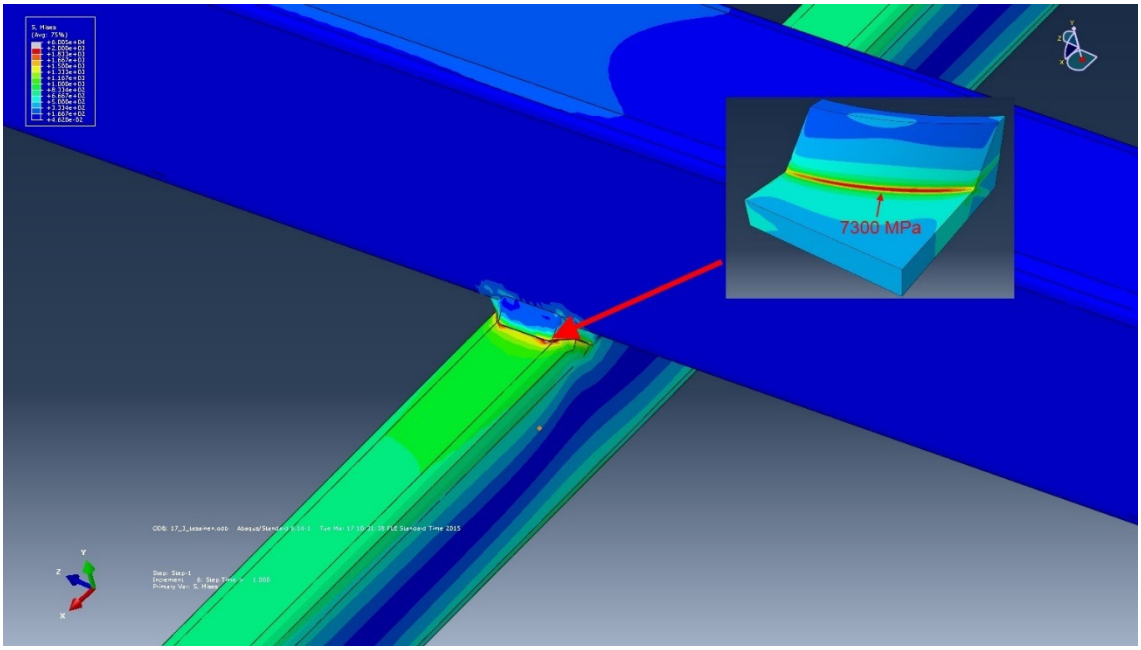

Figure 25. Equivalent stress at the rear weld joint for tarmac flat load case from ENS approach.

Table 10. Equivalent stresses and estimated fatigue lives from ENS approach with S420.

Load case	**Road coating**	**Driven distance [km]**	**Equivalent effective notch stress of driven distance [(MPa/km)$^{1/3}$]**	**Estimated fatigue life for the trailer [km] (FAT 630)**
Flat load	Tarmac	23.5	7300	30 200
	Gravel	20	12000	5 800
Empty trailer	Tarmac	23.5	4500	139 000
	Gravel	20	9100	13 300

For hot spot stress approach the equivalent hot spot stress is determined from the distances of 0.4·t and 1.0·t from the weld toe. In figures 26 and 27 is presented a stress measurement example from hot spot submodel.

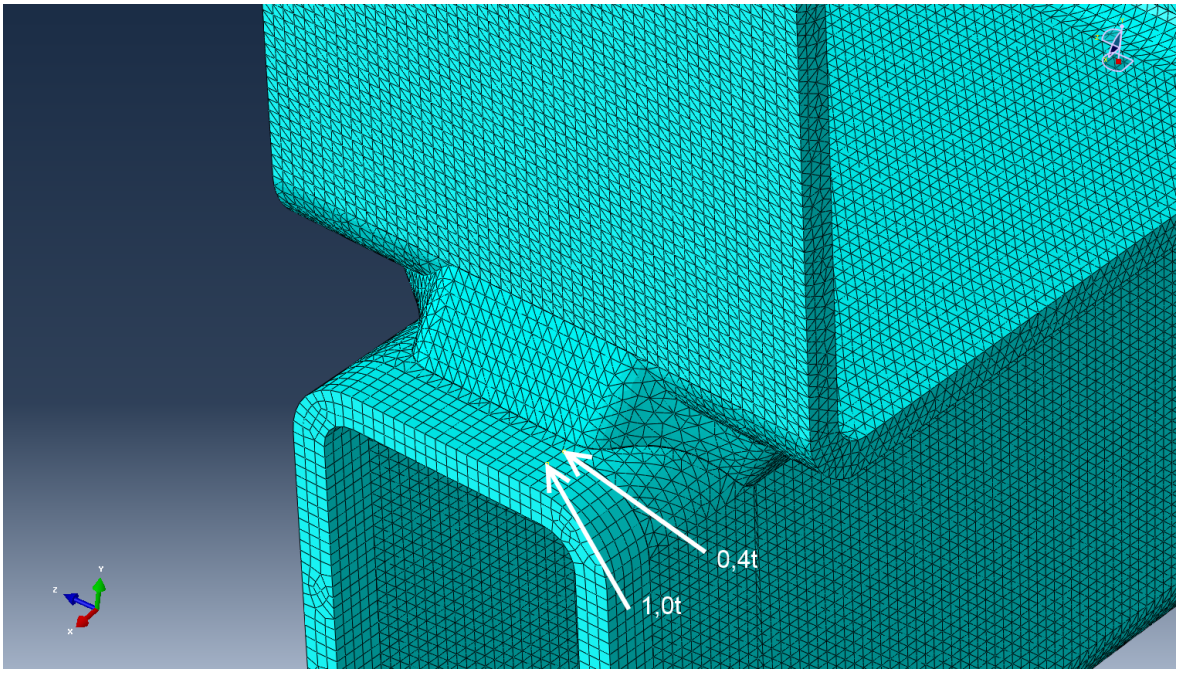

Figure 26. Stress measurement nodes for hot spot stress analysis.

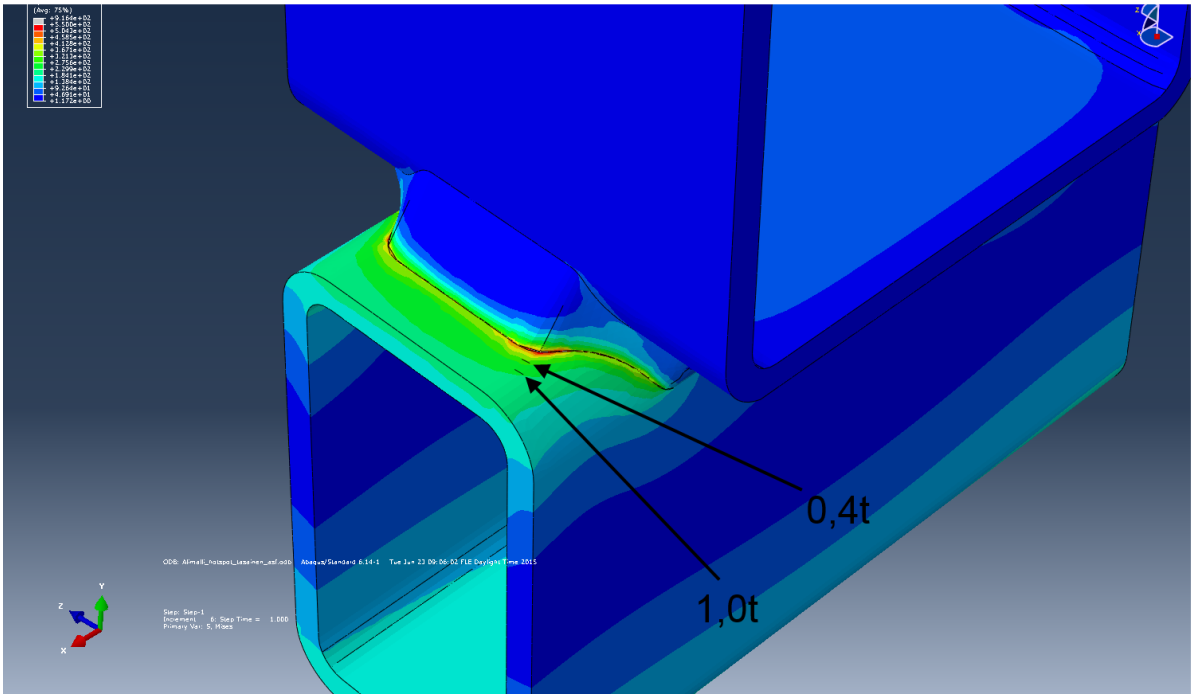

Figure 27. An example of hot spot stress approach analysis.

In Table 11 is presented the equivalent hot spot stresses of the driven distance and calculated fatigue lives according to these equivalent hot spot stresses. These results are later compared to the effective notch stress approach results. It is also later determined which of these approaches is more accurate for this kind of case.

Table 11. Equivalent hot spot stresses and estimated fatigue lives from hot spot stress approach with S420.

Load case	**Road coating**	**Driven distance [km]**	**Equivalent hot spot stress of driven distance [(MPa/km)$^{1/3}$]**	**Estimated fatigue life for the trailer [km] (FAT 100)**
Flat load	Tarmac	23.5	2 100	5 000
	Gravel	20	3 400	1 100
Empty trailer	Tarmac	23.5	1 300	21 000
	Gravel	20	2 300	3 200

5.1.2 Analyses with Form 800

Trailer's frame has to be analyzed also with option material Ruukki's Form 800 rectangular precision tube. Static and fatigue FE-analyses are made also for this Form 800 frame. For Form 800 the thicknesses of profiles are 2 mm. The other dimensions of cross section are the same as in the current trailer. In figure 28 are presented the profiles that are used with this Form 800 precision tube in the trailer. Not all of frame's material is changed to Form 800, only the material of the shaft and transverse beams. Now the material's yield strength is 600 MPa. The equivalent loadings and constraints are set as in the S420 trailer analyses, because no strain gage measurements were carried out with Form 800 trailer to obtain correct equivalent loadings.

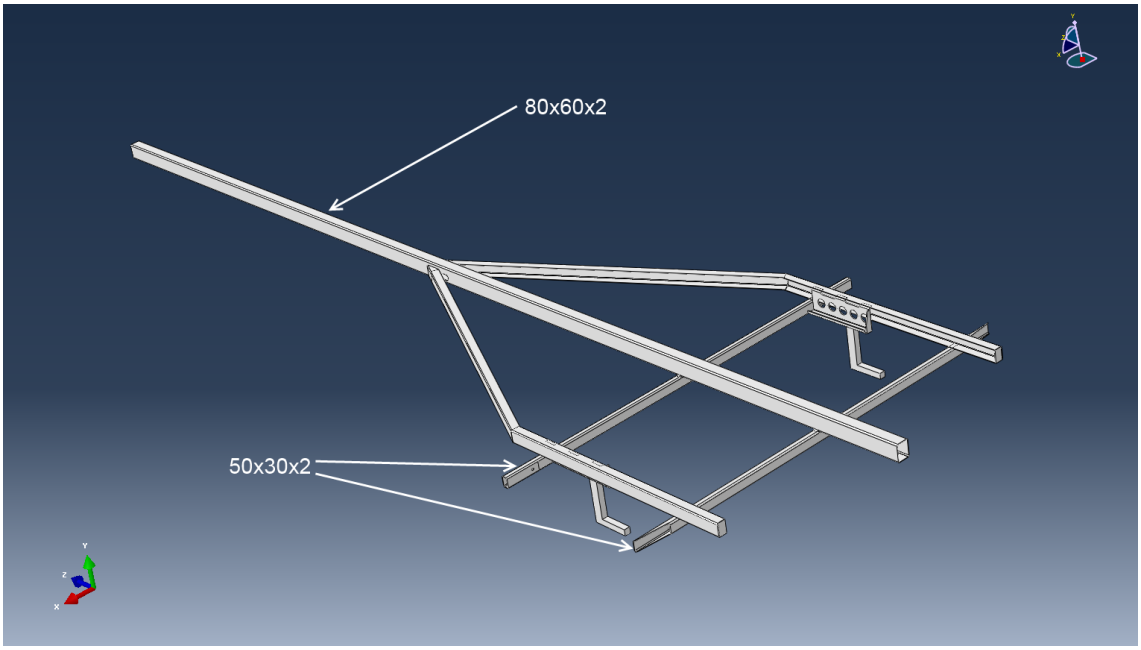

Figure 28. Changed beam profiles from S420 to Form 800.

The most critical location of the structure is the same as with the current trailer. It is the rear weld joint of shaft and transverse beam with all load cases. In figure 29 is presented the stress distribution of the frame with Form 800 precision tubes.

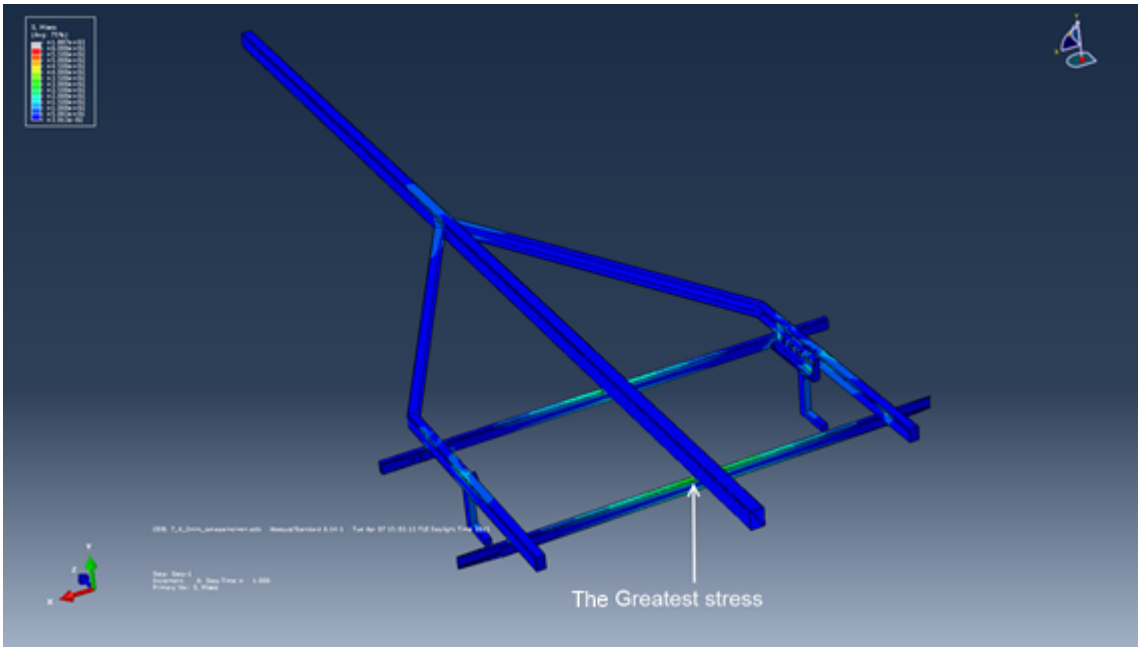

Figure 29. The stress distribution of the trailer's frame with Form 800 and rear-heavy weight load case. Stresses are limited to 600 MPa von Mises stresses.

Closer examinations for rear weld joint are made as for the S420 trailer with submodel, which is shown in figure 30 for rear heavy load case. Submodel is meshed with tetrahedral solid elements.

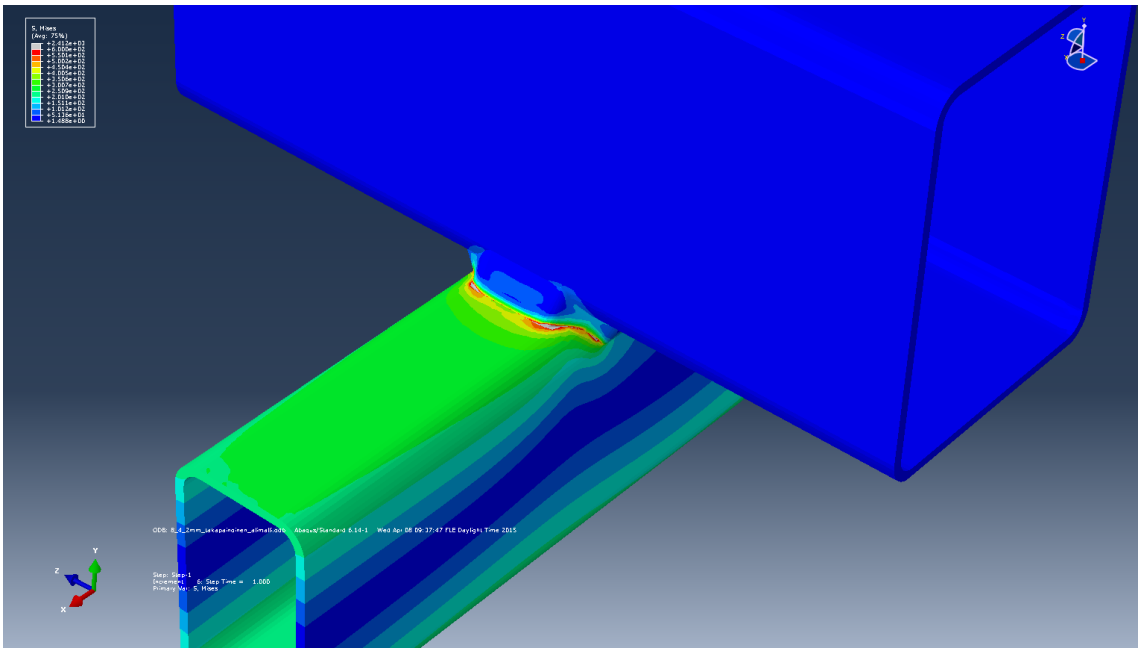

Figure 30. Static rear-heavy weight load case and rear weld joint's stresses. Stresses are limited to 600 MPa von Mises stresses.

Static analysis is made also with greatest overload case (Figure 31.). The loading in this case is set as in the S420 trailer's analysis; to 1170 kg flat load (Appendix III). The results of the Form 800 static analyses are presented in Table 12.

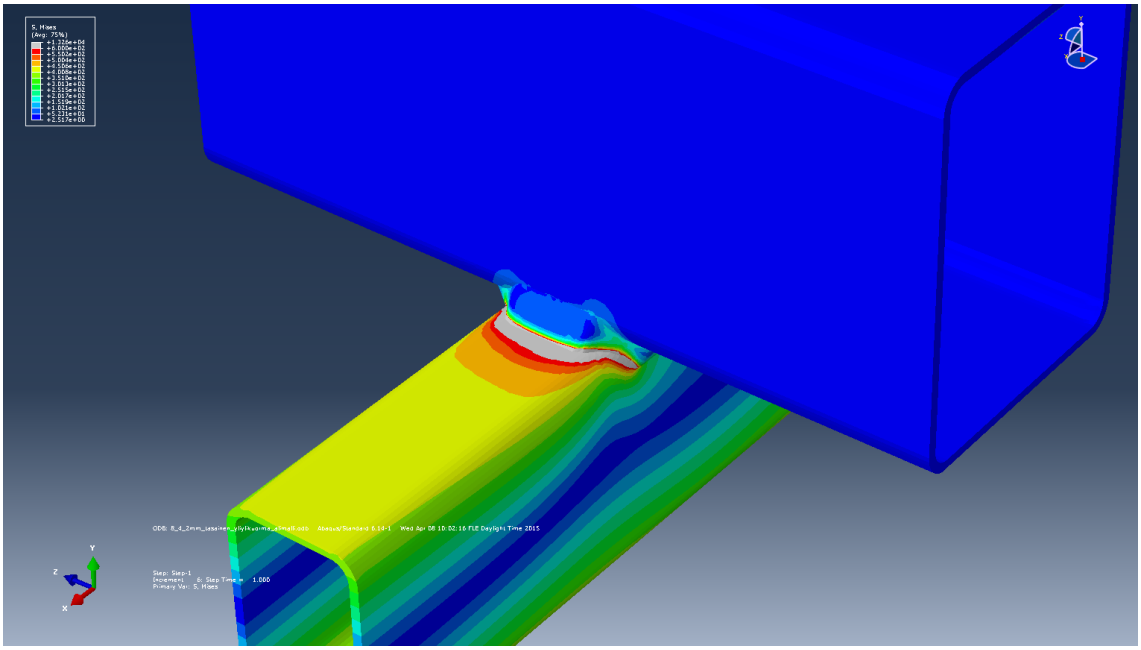

Figure 31. Static greatest overload case and rear weld joint stresses. Stresses are limited to 600 MPa von Mises stresses.

Table 12. Static analysis results with Form 800. The greatest stresses at the rear weld joint's weld toe.

Load case	**Stress at the weld toe [MPa]**
Flat load	700
Front-heavy load	630
Rear-heavy load	750
Greatest overload	1 250

In Table 13 is presented the total deformation of Form 800 trailer. The greatest deformations form in the same location as with the S420 material. This is the location where the U-profiles attach to the trailer's shaft.

Table 13. Total deformations of the trailer with Form 800.

Load case	**Total deformation [mm]**
Flat load	23,3
Front-heavy load	33,5
Rear-heavy load	16,3
Greatest overload	40,3

Fatigue life analyses are made according to the strain gage measurement results of the current trailer geometry and its equivalent stresses. Fatigue analyses are performed as with current material, with ENS and hot spot approaches. In Table 14 is presented the equivalent stresses and calculated fatigue lives for the Form 800 trailer with ENS approach.

Table 14. Equivalent stresses at the weld toe's notch rounding with Form 800 and ENS approach.

Load case	**Road coating**	**Driven distance [km]**	**Equivalent effective notch stress of driven distance [(MPa/km)$^{1/3}$]**	**Estimated fatigue life for the trailer [km] (FAT 630)**
Flat load	Tarmac	23.5	8 000	23 000
	Gravel	20	16 000	2 400
Empty trailer	Tarmac	23.5	5 000	94 000
	Gravel	20	10 000	10 000

The fatigue analysis is made also with hot spot stress approach for this Form 800 trailer as for the S420 trailer. The analysis is made from the same location as with ENS approach. In Table 15 is presented the equivalent hot spot stresses and calculated fatigue lives according to hot spot stress approach.

Table 15. Equivalent stresses at the weld toe from hot spot stress approach with Form 800.

Load case	**Road coating**	**Driven distance [km]**	**Equivalent hot spot stress of driven distance [(MPa/km)$^{1/3}$]**	**Estimated fatigue life for the trailer [km] (FAT 100)**
Flat load	Tarmac	23.5	2 300	3 800
	Gravel	20	4 500	440
Empty trailer	Tarmac	23.5	1 600	11 000
	Gravel	20	3 000	1 500

5.2 Discussion of the FEA results

The equivalent loadings for the FE-models are set according to the strain gage measurements. The static analysis results with current material S420 shows that the trailer will last with each maximum allowed weight load case that is applied on it. The worst load case is the rear-heavy weight load case, which is shown in figure 19. Stresses near the weld toe exceed the yield strength of the material, but that exceeding area is so small that the static strength can be noted to be sufficient. The greatest total deformation with these maximum allowed weight load cases comes from the front-heavy load case and it is approximately 23 mm.

With the greatest overload case, in which the total weight was 1170 kg the stresses are above the material's yield strength. In figure 21 is shown the stress distribution, which shows that stresses exceed considerably the material's yield strength, which is 420 MPa. In figure 21 the gray color near the weld toe means the area, where the stresses exceed yield strength. The total deformation with greatest overload case is 27.8 mm. It was seen with bare eye in strain gage measurement process that this load case deformed greatly the entire trailer structure and it was obvious that it will burden the trailer heavily and the trailer won't probably last very long if it is driven with this load case on it. The difference between the total deformations of front-heavy load case and greatest overload case is not so great because the weight distribution for this greatest overload case was set as flat load.

The static analyses with Form 800 exceed also material's yield strength, which is in this case 600 MPa (Figure 30.). The area where this happens is also small and it can be noted that the static strength is sufficient. As with the current trailer, the greatest overload case form stresses that are way above the maximum allowed and the trailer will probably be damaged soon if taken into use.

The location where the stresses exceed material's yield strength most highly with both of the materials is the rear weld joint. Static stresses with Form 800 compared to the current material S420 are approximately 1.7 times larger at the rear weld joint. The greatest benefit by using Form 800 is the weight reduction that can be achieved when using it in the trailer frame. Problems may however occur from the thin profile wall thicknesses. Trailer might become too flexible. The weight reduction that can be achieved when the shaft's and transverse beam's profiles are changed to 2 mm thicknesses and to Form 800 material is approximately 14.6 kg. It is not much when noticing the trailer's total weight that is 175 kg, but the total weight of the frame is approximately 65 kg so the reduction is over 20 % from the frame. The most of the trailer's total weight comes from the other parts of the trailer for example tires and supports.

When comparing the total deformations between the current S420 trailer and the Form 800 trailer, the deformations are approximately 1.4 times larger with Form 800. If comparing the section modules of these two different profiles, the difference between them is also approximately 1.4. Also the profile thickness of S420 trailer's shaft is approximately 1.4 times thicker than with Form 800 trailer. This means that the calculations are in line with theory. The greater flexibility of the shaft will affect to the trailer's drivability. The trailer will bounce greater and it will also affect to the vehicle that will tow it and might in some cases make the vehicle harder to handle. This is especially when the towing vehicle is lightweight. In Appendix IV is calculated shafts local buckling. Trailer with S420 material has no problem with either of these. With Form 800 material local buckling of the shaft's top flange might become an issue according to calculations, if the shaft is designed to it's yield strength. It is not a problem with this structure. The stresses in the shaft are not close to the yield strength of the material.

The equivalent effective notch stresses in the notch rounding for current trailer are 1.7 times greater on gravel than on tarmac with flat load case. For empty trailer the stresses on gravel are approximately two times greater than on tarmac with S420. The greater difference in results between tarmac and gravel results with empty trailer indicates that the trailer will bounce more heavily when it is empty than with load on it. One reason that will lead for this is the suspension of the trailer. It is designed to work with a boat that weight 570 kilograms and there is no adjust for it, so it will act too stiffly without loading on the trailer. The suspension affects after all greatly to the trailer's fatigue life and it is reasonable to carry a right size boat on the trailer.

The fatigue calculations with ENS approach for the Form 800 trailer are made according to the strain gage measurement of the current material trailer. According to this information the calculated fatigue lives for Form 800 trailer are only indicative. From the results of the Tables 10, 11, 14 and 15 can be formed some estimate cases that would present the normal use of the trailer, however it is hard to tell what is normal use. The average normal use is assumed to contain 100 km of tarmac road and 10 km of gravel road per run. One run is assumed to be performed with boat and one without the boat. The service life prediction in this kind of case is based on assumption that the boat is taken on water in spring and then taken off in autumn. In Table 16 this case is service life prediction 1.

The other service life estimation is made for assumption that some trailer users use their trailer every time they go on water with their boats. This means that the boat rests on the trailer most of the time. This kind of use burdens the trailer much more. The usage may be weekly or even more frequent. This means that the use can be up to 30-50 times or more frequent than in the case, where the trailer is used only two times in a year, in spring and autumn. The service life prediction with this kind of use is 3-5 years with ENS approach. If the usage is this frequent, the driving distances might be shorter than in the first case, so this kind of use where trailer is used 30-50 times in a year with over 100 km driving per run might be an extreme case. In Table 16 this case is service life prediction 2. Equivalent service life predictions in table 16 are made also for the Form 800 trailer, but this estimation is only indicative.

Table 16. Estimated service lives in years with ENS and hot spot stress approaches.

	Service life prediction 1.	Service life prediction 2.
ENS S420 trailer	~ 150 years	~ 3-5 years
Hot spot S420 trailer	~ 25 years	~ 0.8-1.4 years
ENS Form 800 trailer	~ 120 years	~ 2-4 years
Hot spot Form 800 trailer	~ 22 years	~ 0.6-1.1 years

The service life predictions in table 16 are only assumptions and might have nothing to do with the normal use of a trailer. Better way to analyze the service life of a trailer is to analyze the fatigue lives in kilometers from Tables 10, 11, 14 and 15. The static strength of the trailer is sufficient with both S420 and Form 800 trailers. The fatigue life of Form 800 trailer might be the problem despite the sufficient static strength. Because the profiles that have been studied in this work are only thinned (for example 80x60x3 to 80x60x2), the fatigue life of Form 800 will be already worse than with the current trailer and its thicker wall thicknesses of profiles. The vibrations in the trailer will be greater with Form 800 and the thinner profile thicknesses, so the crack growth will be therefore greater also. The fatigue calculation results give some knowledge of this point, even they are made according to the strain gage measurement data of the current trailer. The fatigue life will be shorter with Form 800 than with S420 due to stress ranges that are greater with it. The fatigue life of Form 800 trailer in relation to S420 trailer should follow roughly the equation:

$$N_{Form\ 800} = \left(\frac{t_{Form\ 800}}{t_{S420}}\right)^3 \tag{9}$$

In equation 9 the $t_{Form\ 800}$ is the wall thickness of the tube profile of Form 800 trailer, t_{S420} is the wall thickness of the tube profile of S420 trailer and $N_{Form\ 800}$ is the fatigue life of Form 800 trailer. If more accurate results are needed, a prototype of Form 800 trailer is good to be made and strain gage measurements taken from the trailer as it was taken from the current S420 trailer. To achieve the fatigue life of Form 800 trailer as good as with the S420 trailer, the shapes of the profiles need to be changed also.

When comparing the fatigue life calculation results from ENS and hot spot stress approaches, the hot spot stress approach gives shorter fatigue life predictions than ENS approach with S420 material. With Form 800 material the difference is even greater. The comparison of ENS and hot spot approaches is presented in table 17. With empty trailer case on tarmac, the difference between ENS and hot spot results are smallest. The greater the equivalent stresses are, the greater is the difference between the results from these two approaches. This can be seen when comparing the results between S420 and Form 800 fatigue lives. The location where the equivalent stresses are measured from is not in the straight part of the weld but its corner, where the lower beam's corner starts. The equivalent notch stress can be determined straight from the notch, so no extrapolation is needed. Sometimes if the geometry is complicated, measuring the hot spot stress correctly can be challenging.

Table 17. ENS and hot spot approach equivalent stress and fatigue life comparison.

	ENS	Hot spot	**Difference**	ENS	Hot spot	**Difference**
	Equivalent stress [MPa]			Fatigue life [km]		
S420, Flat load, tarmac	7 300	2 100	**3.4**	30 200	5 000	**6.0**
S420, Flat load, gravel	12 000	3 400	**3.5**	5 800	1 100	**5.3**
S420, Empty trailer, tarmac	4 500	1 300	**3.5**	139 000	21 000	**6.6**
S420, Empty trailer, gravel	9 100	2 300	**3.9**	13 300	3 300	**4.0**
From 800, Flat load, tarmac	8 000	2 200	**3.6**	23 000	3 600	**6.2**
Form 800, Flat load, gravel	16 000	4 500	**3.6**	2 400	440	**5.5**

Table 17. Continues.

	ENS	Hot spot	**Difference**	ENS	Hot spot	**Difference**
	Equivalent stress [MPa]			Fatigue life [km]		
Form 800, Empty trailer, tarmac	5000	1 600	**3.1**	94 000	11 000	**8.5**
Form 800, Empty trailer, gravel	10 000	3 000	**3.3**	10 000	1 500	**6.7**

There have been also no reclamations from the trailer users that the trailer has been damaged from its frame's weld joints. If the fracture happens in the weld joint, it might after all not be noticed instantly. The trailer might last with fracture in the other weld joint until also the other weld joint fractures.

ENS approach seems to be the better method to use with this case. From these two approaches and the results they give the ENS approach seems to be the more accurate in this case. In ENS approach the notch is modelled at the weld toe and root, which gives straightly the stress value from where it is wanted. With hot spot stress approach the stress is extrapolated to the weld toe, which can cause some inaccuracy to the results. Also the equivalent stresses are form great, which seems to cause inaccuracy with hot spot approach. ENS approach needs more work than hot spot approach, because the weld and the notch need to be modelled properly. The benefits of hot spot approach are that analyses can be performed also for medial surface shell element models and with coarser meshes. This makes it faster method and therefore it can be famous method in industry. If the location where the equivalent stresses need to be measured is complex or the weld root is the critical location, the ENS approach is the one to be used.

6 CONCLUSIONS

Strength analysis was made from the current trailer, which is manufactured from S420 structural steel. For more economical and sustainable solution, the trailer's material is planned to change to high strength steel. The main advantage from this material change is that the weight of the trailer can be reduced. Strength analysis is made also with high strength steel trailer to determine if it is reasonable to change the material.

The weight reduction that can be achieved by narrowing the profiles is not more than approximately 15 kilograms. The total weight of the trailer is 175 kilograms so the total weight reduction is not very significant. The weight of the current trailer's frame is approximately 65 kg, so the weight reduction from the frame is approximately 20 %. This can be noted to be quite considerable. If greater weight reduction is attempted, the change has to be made for other parts of the trailer also. The heaviest parts of the trailer are the tires and supports that support the trailer from below. From these parts more weight reduction can be achieved.

If the material is changed to high strength steel and the profiles are chose to be thinned, the manufacturing process need some changed also, for example the welding process. This is something that will cause some additional expenses. The changed material can be applied to other trailer models also, but it will be good to perform same kind of analyses that was made from the trailer in this work and also prototype testing. This is again something that will cause expenses.

The current profiles are 3 mm thick, so decreasing the wall thicknesses of the profiles to 2 mm might cause problems especially to the shaft, which might become too flexible. From the analytical calculations in Appendix IV, the flexibility of the trailer is not a problem with Form 800. Problems can however become with the local buckling of the shaft with this material, if the shaft will be designed to material's yield strength. However, the FEA presented that the stresses in the shaft will not be close to material's yield strength if proper loads are used, consequently local buckling is not critical for both of these trailers. The most secure way to test the Form 800 trailer is to make a prototype and to analyze the functioning with it. It might not be good for the business, if the trailer looks too flexible when loaded, even if

it will last easily the loads that are set on it. Some trailer users might not mind the weight of the trailer. They want only a trailer that looks like it will last. If there is a change to take a narrower and higher profile, for example 90x50x2 in to account, the section modulus will be greater in the loading direction compared to 80x60x2 profile. This means that the trailer won't deform so greatly and it will be more stable.

Trailer's fatigue life will be shorter with Form 800. This is because the profiles are only thinned compared to the S420 trailer. This was also seen from the fatigue calculations. The fatigue life of the Form 800 trailer should follow the equation 9. In this case there is a difference between the results of FEA and equation 9. If proper fatigue life of the Form 800 trailer is needed, same kind of strain gage measurements is good to be done from Form 800 trailer as was done from S420 trailer in this work.

Trailer users can increase the fatigue life and therefore the service life of the trailer if the trailer is loaded with front-heavy loading. This load case will form the greatest deformation in the shaft, but according to the strain gage measurement the stress changes with front-heavy loading will be smaller with this kind of loading. In other words, the trailer will be more stable with front-heavy loading when driven. Also the rear-heavy loading is better than flat loading, which seems to be the worst load distribution for the trailer in fatigue perspective.

Strain gage measurements showed that it is almost as stressful to the trailer to drive it empty than with load on in. Especially the equivalent stresses from the empty trailer and front-heavy load cases are quite close each other especially on tarmac coating. The material change to Form 800 depends how long guarantee is planned to give for the trailer. The fatigue life and therefore the service life of the trailer are dropped if the change is made and the profiles used are the same as in the S420 trailer. If the fatigue life for Form 800 trailer needs to be increased, other profiles have to be taken into account. The wall thicknesses of profiles are good to retain in the original 3 mm and make the changes to other dimensions of the profile. Profile's wall thickness has a great role to the fatigue strength.

The ENS approach in this kind of application seems to be more accurate method to use than the hot spot stress approach. In ENS approach the rounding is modelled to the examined

weld geometry, so it takes into account the notch effect in the geometry also. The difference in equivalent stresses between ENS and hot spot stress approaches is 3.1…3.9. The greater the equivalent stresses are, the greater is the difference between ENS and hot spot approaches. The difference between the approaches decreases when the equivalent stresses are smaller. This indicates that the hot spot tress approach is not good method to use with great equivalent stresses. From these conclusions and the fact that no reclamations has been had that the trailer has failed from its rear weld joint in use, the ENS approach seems to be more accurate method to use with this kind of geometry.

If the analyzed geometry is complex, the use of ENS requires right kind of FEA-software. In this thesis the used softwares were Femap and Abaqus. Femap is good software for medial surface modelling, but when solid and hexahedral elements are need to used, the Abaqus was the right program to use. With Femap, modelling a submodel is hard and much experience is needed to make a proper submodel with it. Submodels are important when exact mesh is needed and the number of elements is growing large. With Abaqus, submodelling and hexahedral meshing was easier.

The fatigue life of structure's weld joints can be increased by many techniques. One of these, and the easiest to perform is the grinding of the weld toe or remelting it with plasma or TIG-dressing. The residual stresses have an important role in this kind of case, where the structure is also immersed in to the zinc bath. Residual stresses can be decreased at the weld toes by for example hammer peening. This method however is harder to perform and it will require experience to be performed properly. The easiest way to increase the fatigue life however is to aim as good weld quality as possible. This means that the welding parameters and additives are proper and optimized. This will require also a good quality inspection process, which reveals the low quality welds in the manufacturing process.

For future researches, the effect of hot dip galvanization to high strength steels used in the trailer need to be investigated. In researches liquid metal embrittlement has been found out to decrease greatly the fatigue life of hot dip galvanized high strength steel structures. This is important if the trailer's material is changed to high strength steel. Also same kind of strain gage measurements from the possible Form 800 prototype trailer is good to be done to determine the real stress state from the new structure and the real fatigue life of this new trailer.

SOURCES

Berchem, K. & Hocking, M.G. 2006. The influence of pre-straining on the high-cycle fatigue performance of two hot-dip galvanized car body steels. Materials characterization, Vol. 58, Iss. 7. pp. 593-602.

Björk, T. 2015. Doctor of Science in Technology. Professor of Steel Structures. Lappeenranta University of Technology. Private discussions 01.05.2015 & 06.08.2015.

Carpio, J., Casado, J.A., Álvarez, J.A., Méndez, D. & Gutiérrez-Solana, F. 2010. Stress corrosion cracking of structural steels immersed in hot-dip galvanizing baths. Engineering Failure Analysis. Vol. 17, Iss. 1. University of Cantabria. pp. 19-27.

Dowling, N. 2007. Mechanical behavior of materials. Third edition. Upper Saddle River (NJ): Prentice Hall. 912 p.

Feldmann, F., Schäfer, D., Bleck, W., Durst, A., Pohl, M., Luithle, A., Schütz, A., Trieber, J., Vormwald, M., Versch, C., Berger, C., Landgrebe, R., Adelmann, J., Körber, D., Keitel, S., Schmeink, H. & Nüsse, G. Forschungsvorhaben P766. Technologie und Sicherheitsgewinnung beim Feuerverzinken zum Ausbau der Marktpositi-on des verzinkten Stahlbaus. Düsseldorf: Verlag und Vertriebsges. 259 p.

Fricke, W. 2013. IIW Guideline for the assessment of weld root fatigue. Weld world. International Institute of Welding. DOI 10.1007/s40194-013-0066-y. pp. 753-791.

Gang, S., Huiyong, B. & Bijlaard, S.K. 2012. Tests and numerical study of ultra-high strength steel columns with end restraints. Journal of Constructional Steel Research. Vol. 70. pp. 236-247.

Gangloff, P. 2003. Hydrogen assisted cracking of high strength alloys. Comprehensive Structural Integrity. Department of Materials Science and Engineering. University of Virginia. 194 p.

Hannah, R.L. & Reed, S.E. 1993. Strain gage user's handbook. First edition. Chapman & Hall. 465 p.

Hobbacher, A. 2008. Recommendations for Fatigue Design of Welded Joints and Components. International Institute of Welding. IIW-Document XIII-2151r4-07. 142 p.

Ikonen, K. & Kantola, K. 1991. Murtumismekaniikka. Second edition. Espoo: Otatieto Inc. 413 p.

Ilvonen, R., Kähönen, A., Siljander, A. & Pärssinen, V. 2008. Putkipalkkien ja korkealujuuksisten terästen käyttö ajoneuvorakenteissa. VTT release. Espoo: Valtion Teknillinen Tutkimuskeskus. 44 p.

Kinstler, T.J. 2010. Current knowledge of the cracking of steels during galvanizing. A Synthesis of the Available Technical Literature and Collective Experience for the American Institute of Steel Construction. GalvaScience LLC. 79 p.

Konstruktiotekniikan mittaukset – vastusvenymäliuskamittaukset. 1993. 41 p.

Mendala, J. 2012. Liquid metal embrittlement of steel with galvanized coatings. Department of Materials Technology, Silesian University of Technology. Katowice, Poland. [web document]. [Cited: 14.1.2015]. Available: http://iopscience.iop.org/1757-899X/35/1/012002/pdf/1757-899X_35_1_012002.pdf.

Niemi, E. & Kemppi, J. 1993. Hitsatun rakenteen suunnittelun perusteet. Painatuskeskus Inc. 337 p.

Niemi, E., Kilkki, J., Poutiainen I. & Lihavainen V. 2004. Väsymättömän hitsausliitoksen suunnittelu. Fourth edition. LTY Digipaino, 138 p.

Ruukki. Rakenneputket. [Ruukki's website]. 2014. [Cited: 10.8.2015]. Available: http://www.ruukki.fi/Teras/Rakenneputket

Ruukki. Ohutseinämäputket. [Ruukki's website]. 2014. [Cited: 10.8.2015]. Available: http://www.ruukki.fi/Teras/Ohutseinaputket-EN-10305-standardin-mukaan

Ongelin, P. & Valkonen, I. Rakenneputket. EN 1993-Käsikirja. 2012. Otavan Kirjapaino Inc. Keuruu. Rautaruukki Inc. 684 p.

Suomen kuumasinkitsijät ry. General instruction. 2007. Kuumasinkityksen toimintaketju. General instructions. [Cited: 20.1.2015]. Available: http://www.kuumasinkitys.fi/kuumasinkityksen_toimintaketju_yleisohje_1_2007.pdf.

Sperle, J. 1997. High strength sheet and plate steels for optimum structural performance. [Web document]. Borlänge, Sweden: SSAB. 13 p. [Cited 20.1.2015]. Available: http://www.sperle.se/referenser/pdf/artiklar/V2_JK250.pdf

Swanger, H. & France, R. Effect of zinc coatings on the endurance properties of steel. 1933. National Bureau of Standards. Vol. 9. 851 p. [Cited 16.4.2015]. Available: http://nvlpubs.nist.gov/nistpubs/jres/9/jresv9n1p9_A2b.pdf

Vidensky, I.V., Shchukin, E.D., Savenko, V.I., Petrova, I.V. & Polukarova. Z.I. 1998. Liquid metal embrittlement in the absence of liquid metal phase: in studies of surface damageability and in hard materials machining. Colloids and Surfaces A: Physicochemical and Engineering Aspects. Institute of Physical Chemistry. Russian Academy of Sciences. Vol. 156. pp. 349-355.

Wei, S. 2013. Steels. From materials science to structural engineering. Springer-Verlag London. 278 p.

Measurement plan

1. Finite element analysis with FEMAP

- A simple medial surface model was created to determine the most critical locations of the structure.
- Loading for the model was set according to Majava Group's report (Figure 1).

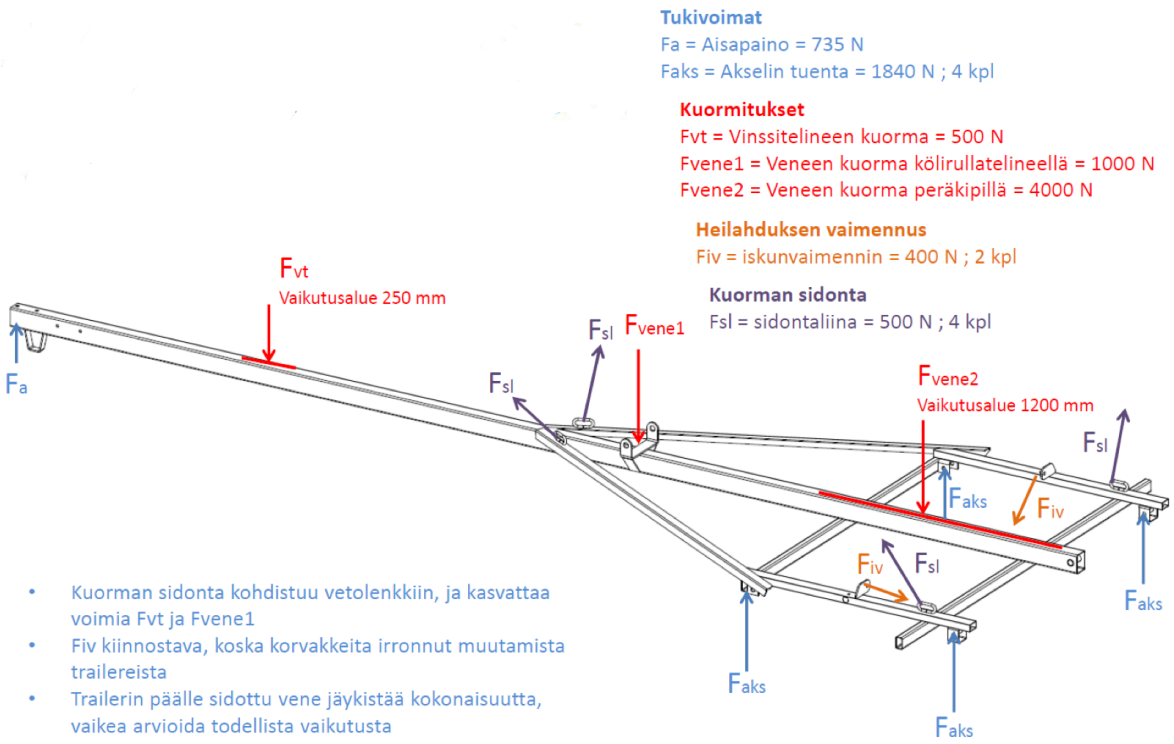

Figure 1. Loading of the trailer.

The results from FEA are shown in figures 2-4. The most critical location of the structure is the rear weld joint.

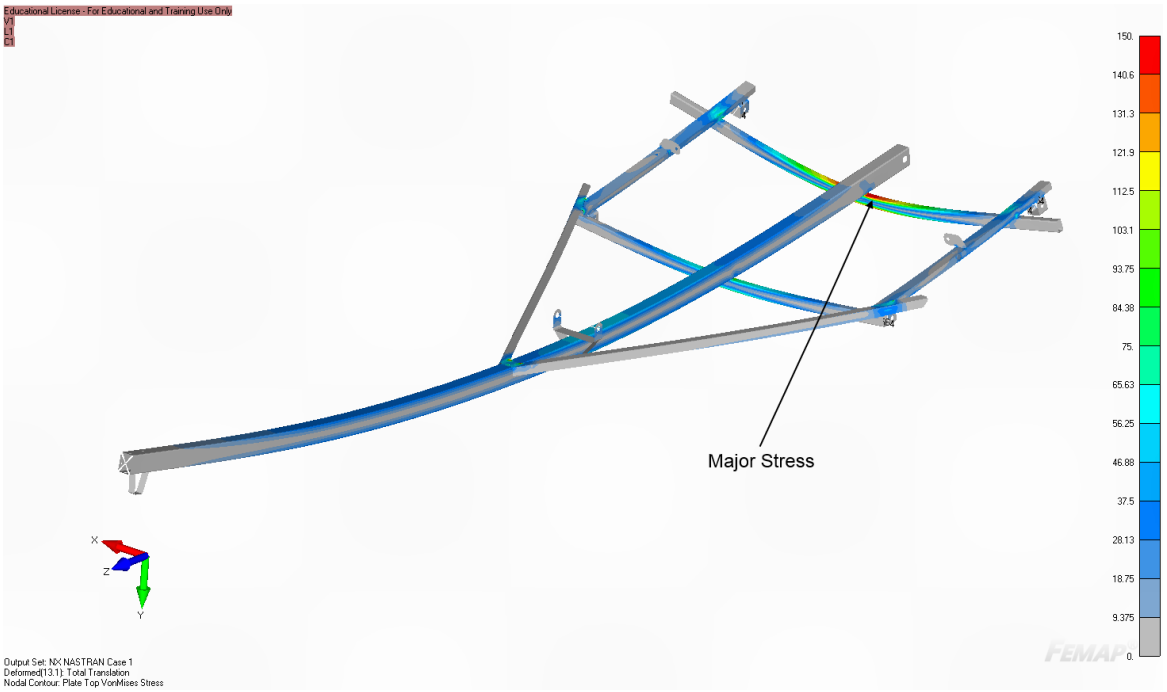

Figure 2. Stress distribution.

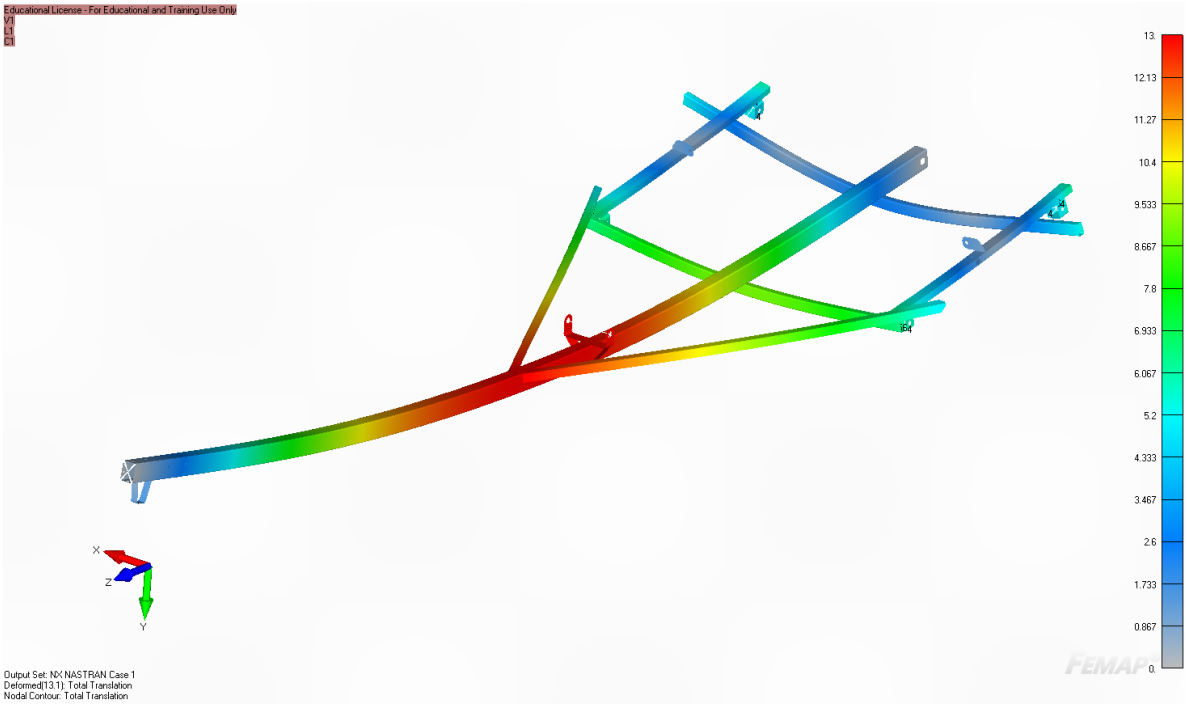

Figure 3. Total deformation.

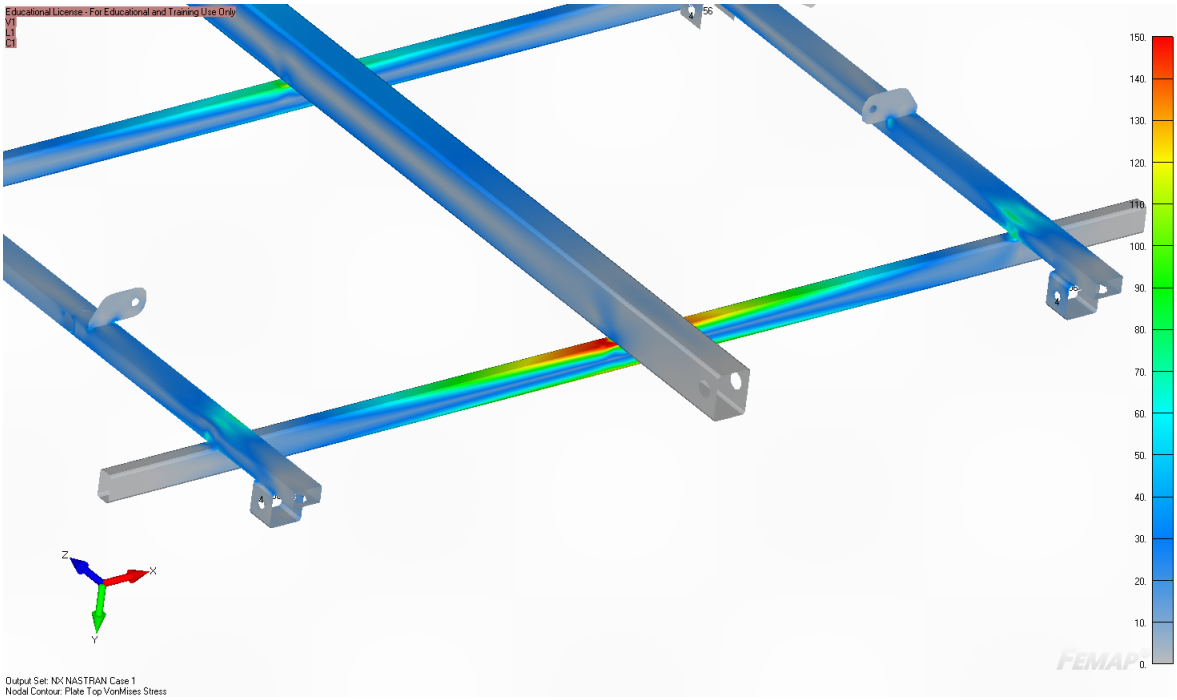

Figure 4. The most critical location of the structure.

2. Strain gage locations

According to FEA the greatest stresses form into the two weld joints of shaft and transverse beams. Bending stresses will be measured from these locations. (Figure 5.)

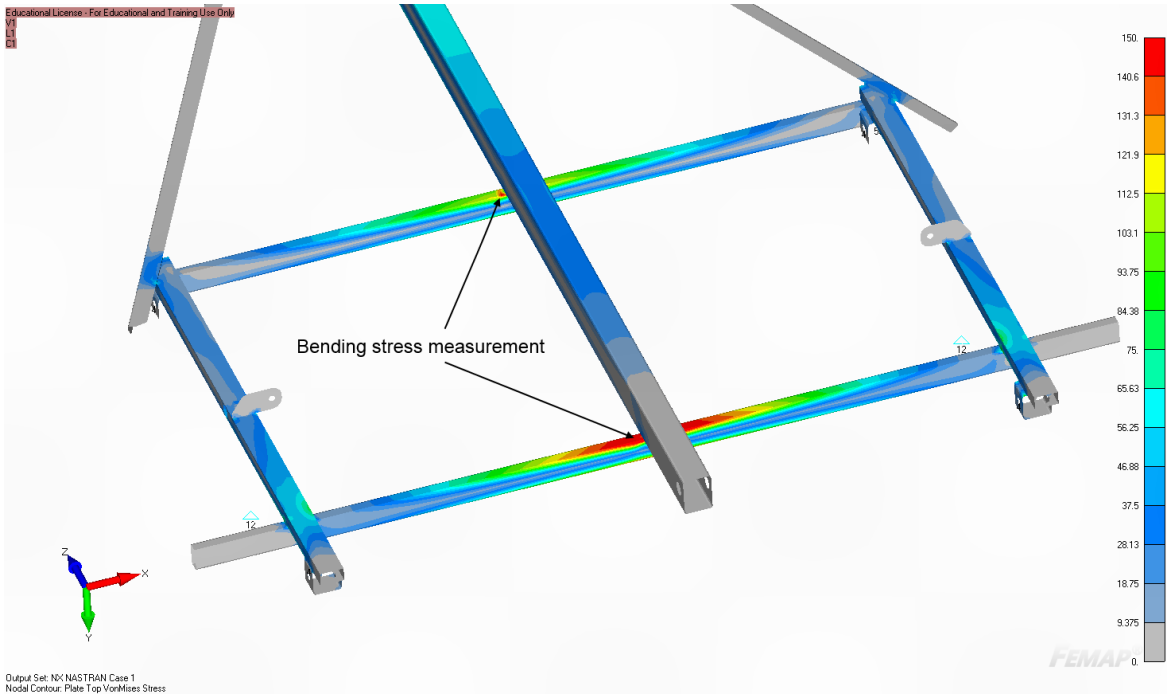

Figure 5. Bending stress measurement near the weld joints.

From the rear weld joint a hot spot measurement will be made. (Figure 6.)

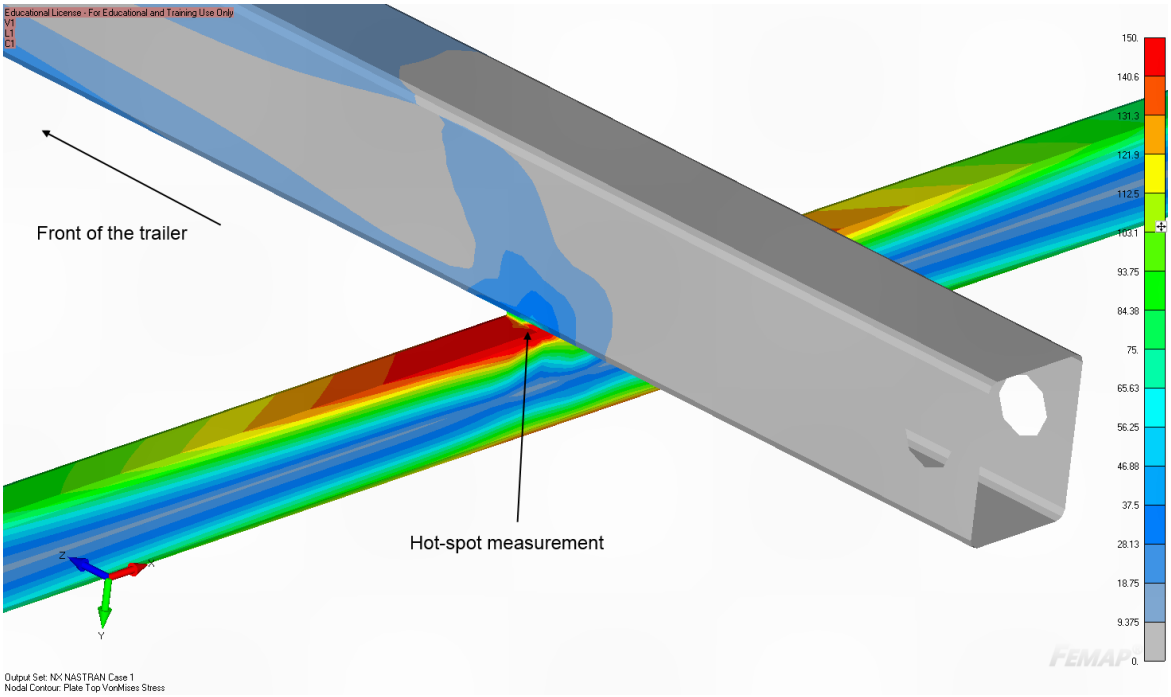

Figure 6. Hot spot measurement from the rear weld joint.

The maximum deformation is located at the center of the shaft. From this location a bending moment and axial force measurement will be made. (Figure 7.)

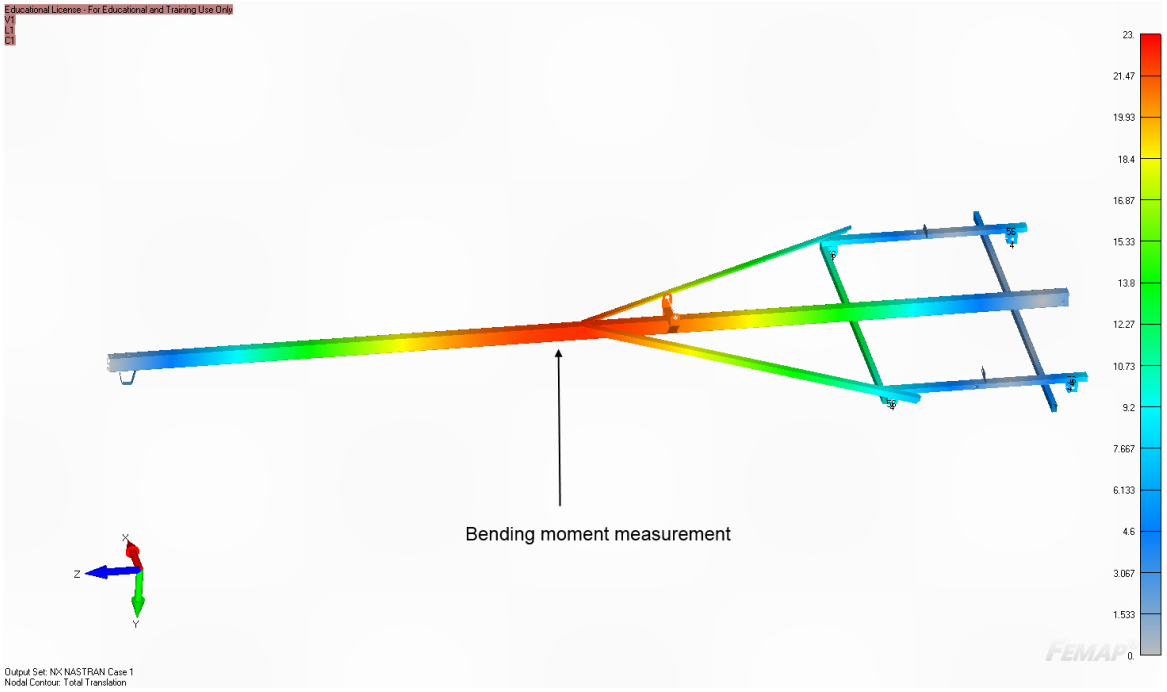

Figure 7. Bending moment measurement.

According to initial information, the lugs that attach the suspension to the frame have been loosen in some cases. Hot spot-measurement will be made near the weld of the lug. (Figure 8.)

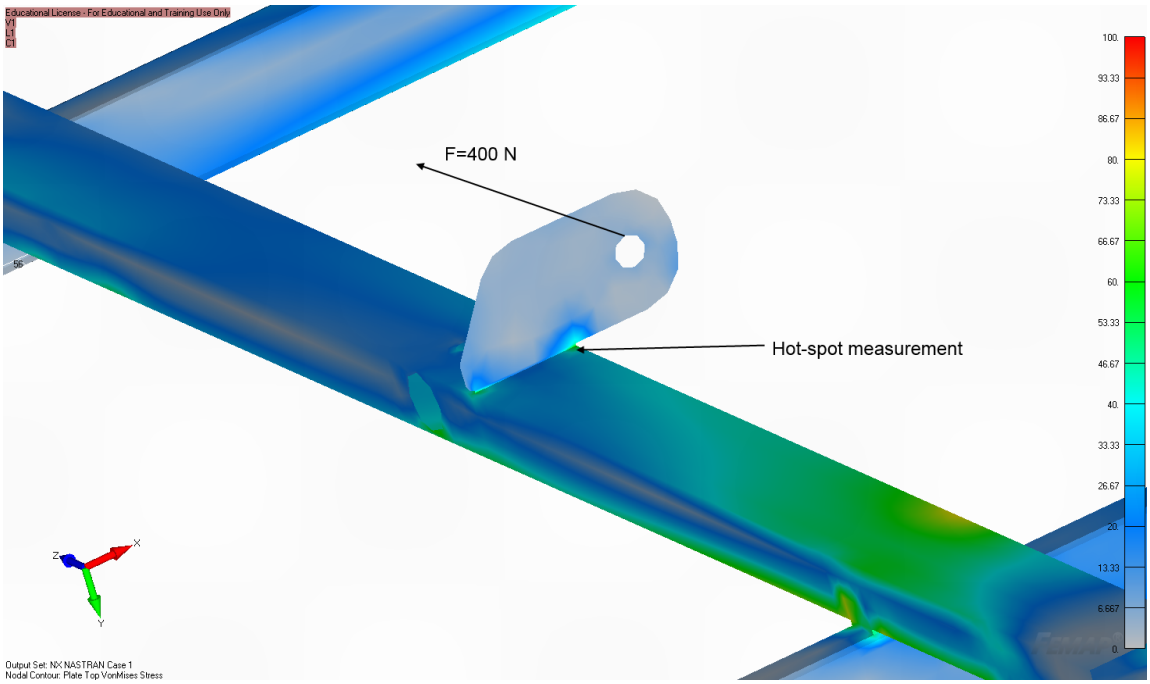

Figure 8. Hot spot measurement from the lug.

Summary of measurement locations:

Strain gage number	Location of the strain gage.
1.	Strain gage at the distance of 0.4t from the rear weld joint of shaft and transverse beams. (Figure 5.)
2.	Strain gage at the distance of 0.4t from the front weld joint of shaft and transverse beams. (Figure 5.)
3.	Hot spot measurement from rear weld joint. (Figure 6.)
4.	Bending moment measurement from the shaft. (Figure 7.)
5.	Hot spot measurement from the suspension lug. (Figure 8.)

3. Measurement implementation

Stage 1: Strain gages will be reseted when the trailer lies on its own weight, because the weight of the trailer is not significant and the effect to results will be small.

Stage 2: Test drive with empty trailer.

Stage 3: Lifting the boat on the trailer. The boat should be maximum weight to get the maximum allowed combination weight, which is 750 kg.

Stage 4: Static measurements from the boat and trailer combination with different load cases.

Stage 5: Test drive route that will include different kind of roads and driving speeds. The routes are now covered with snow, so the test drive route has to be planned so that it corresponds as much as possible to summer conditions. Test drives will be performed with different load cases.

Stage 6: Obstacle overrun. This stage will be completed by throwing a wood plank under the trailer when it is moving approximately 20 km/h. Two different cases will be investigated, wooden plank under both of the tires and wooden plank under the other tire. This will be performed with different load cases.

Stage 7: Dropping the boat from the trailer.

APPENDIX II

Measurement stages.

No.	**Stage**	**Content**	**Total weight**	**Duration**
1.1	Calibration	Strain gage calibration	-	-
2.1	Static measurements	Trailer with empty boat	448 kg	2.0 min.
2.2	Static measurements	Trailer with empty boat and motor	548 kg	2.0 min.
2.3	Static measurements	Flat load	750 kg	2.0 min.
2.4	Static measurements	Rear-heavy load	750 kg	2.0 min.
2.5	Static measurements	Front-heavy load	750 kg	2.0 min.
2.6	Static measurements	Flat overload	1000 kg	2.0 min.
2.7	Static measurements	Flat greatest overload	1170 kg	2.0 min.
3.1	Test drive	Flat load	750 kg	45 min.
3.2	Test drive	Rear-heavy load	750 kg	45 min.
3.3	Test drive	Front-heavy load	750 kg	45 min.
3.4	Test drive	Empty trailer	178 kg	45 min.
4.1	Lifting and dropping on the snow bank	Front-heavy load	750 kg	5 min.
4.2	Lifting and dropping on the snow bank	Rear-heavy load	750 kg	5 min.

Results from static strain gage measurements.

Load case	**Stresses [MPa]**					
	SG1	**SG2**	**SG3**	**SG4**	**SG5A**	**SG5B**
Trailer with empty boat	-166.4	-123.4	-21.7	44.5	-40.2	37.3
Trailer with empty boat and motor	-191.1	-147.3	-27.0	33.5	-31.9	28.9
Flat load	-235.4	-178.3	-30.3	47.5	-58.9	56.5
Front-heavy load	-226.1	-157.4	-29.7	55.4	-92.7	90.3
Rear-heavy load	-238.4	-208.1	-30.9	15.5	-25.5	22.9
Flat overload	-283.2	-219.6	-31.0	60.1	-97.3	95.1
Flat greatest overload	-320.0	-250.2	-36.1	58.5	-104.4	102.5

Results from test drives. Equivalent stresses according to the stress history.

Load case	**Equivalent stresses [MPa]**				
	SG1	**SG2**	**SG3**	**SG4**	**SG5AB**
Tarmac, Flat load	1378	1293	347	495	564
Tarmac, Rear-heavy load	1047	1241	428	982	650
Tarmac, Front-heavy load	1005	1057	288	374	381
Tarmac, Empty trailer	841	878	334	525	292
Gravel, Flat load	2752	2217	748	894	1031
Gravel, Rear-heavy load	2035	2117	713	1405	982
Gravel, Front-heavy load	1957	2059	530	768	664
Gravel, Empty trailer	1677	1601	668	1000	508
Combined tarmac and gravel, Flat load	2863	2355	773	942	1085
Combined tarmac and gravel, Rear-heavy load	2123	2251	761	1477	1069
Combined tarmac and gravel, Front-heavy load	2042	2148	557	796	703
Combined tarmac and gravel, Empty trailer	1745	1685	695	1046	538

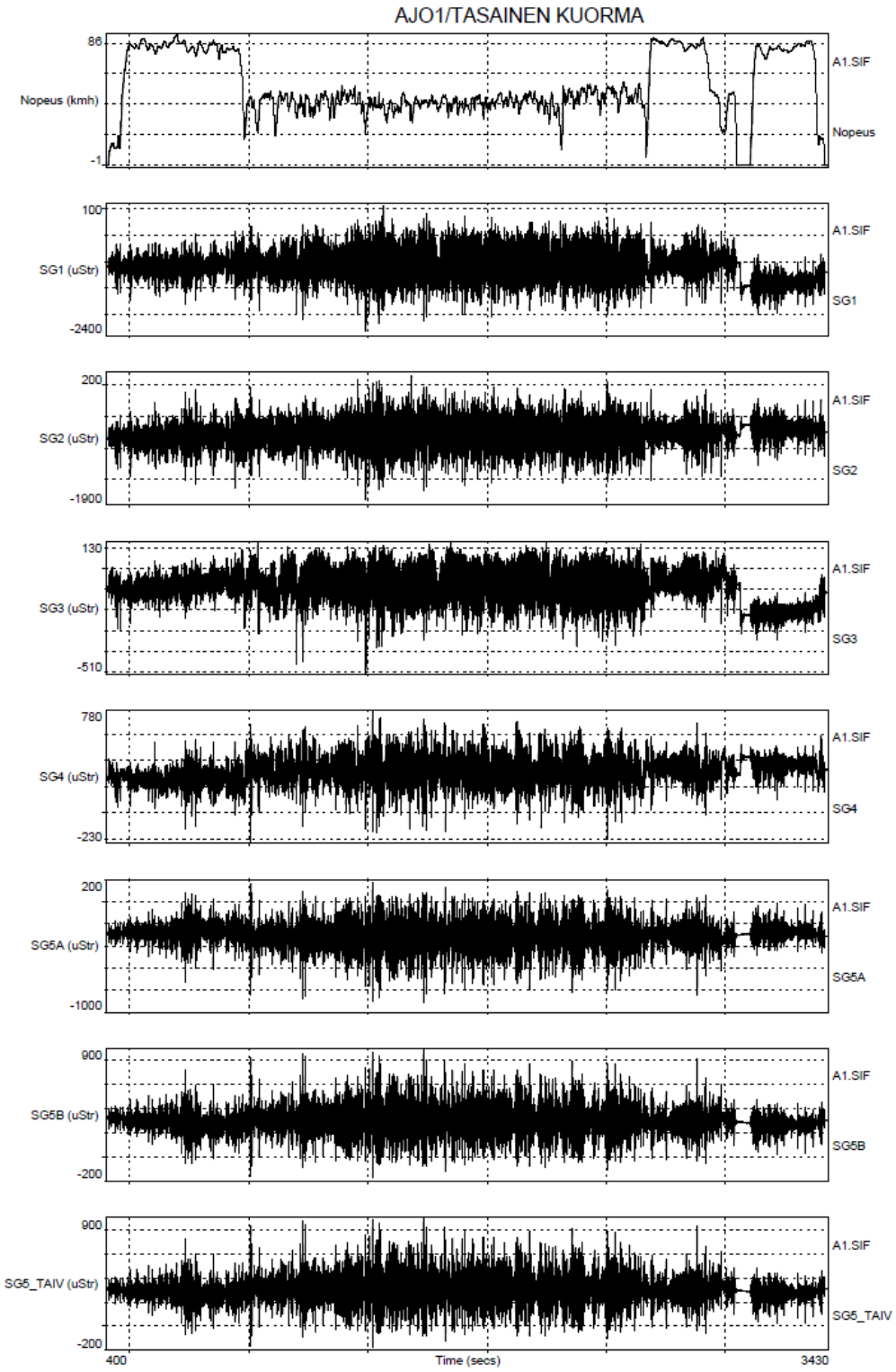
AJO1/TASAINEN KUORMA
86
Nopeus (kmh)
-1
A1.SIF
Nopeus
100
SG1 (uStr)
-2400
A1.SIF
SG1
200
SG2 (uStr)
-1900
A1.SIF
SG2
130
SG3 (uStr)
-510
A1.SIF
SG3
780
SG4 (uStr)
-230
A1.SIF
SG4
200
SG5A (uStr)
-1000
A1.SIF
SG5A
900
SG5B (uStr)
-200
A1.SIF
SG5B
900
SG5_TAIV (uStr)
-200
A1.SIF
SG5_TAIV
400
Time (secs)
3430

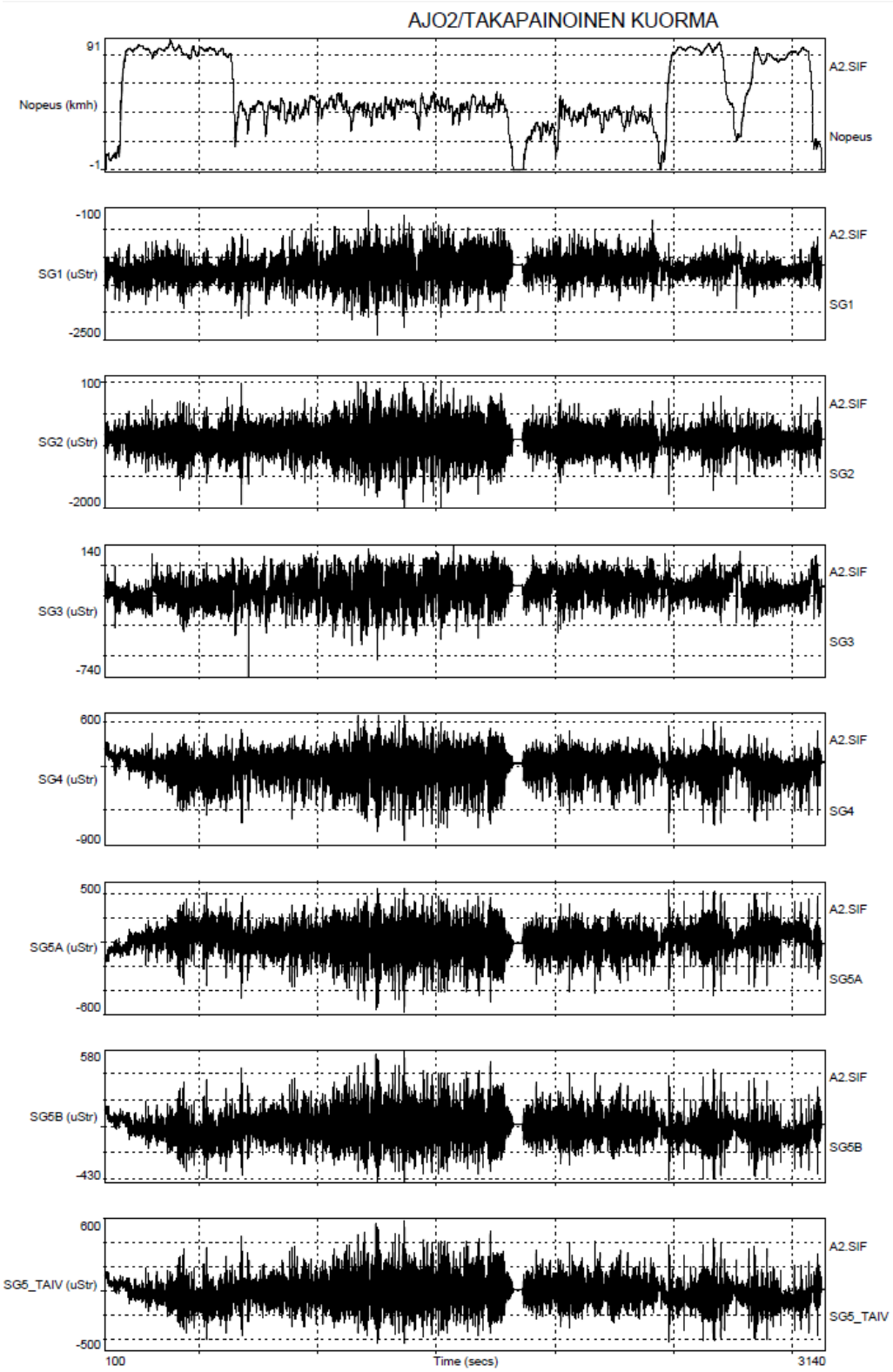
AJO2/TAKAPAINOINEN KUORMA
91
Nopeus (kmh)
-1
A2.SIF
Nopeus
-100
SG1 (uStr)
-2500
A2.SIF
SG1
100
SG2 (uStr)
-2000
A2.SIF
SG2
140
SG3 (uStr)
-740
A2.SIF
SG3
600
SG4 (uStr)
-900
A2.SIF
SG4
500
SG5A (uStr)
-600
A2.SIF
SG5A
580
SG5B (uStr)
-430
A2.SIF
SG5B
600
SG5_TAIV (uStr)
-500
A2.SIF
SG5_TAIV
100
Time (secs)
3140

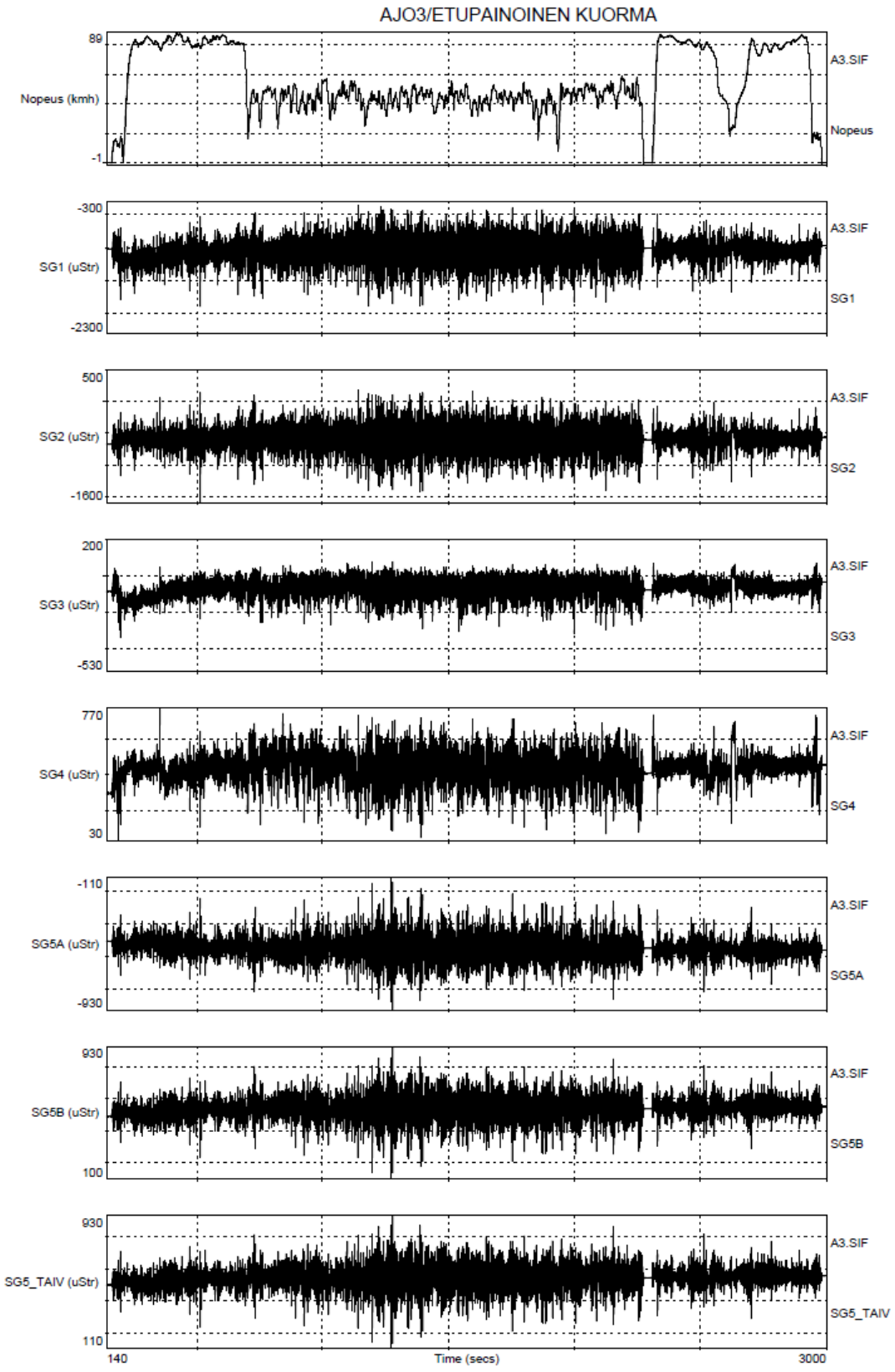
AJO3/ETUPAINOINEN KUORMA
89
Nopeus (kmh)
-1
A3.SIF
Nopeus
-300
SG1 (uStr)
-2300
A3.SIF
SG1
500
SG2 (uStr)
-1600
A3.SIF
SG2
200
SG3 (uStr)
-530
A3.SIF
SG3
770
SG4 (uStr)
30
A3.SIF
SG4
-110
SG5A (uStr)
-930
A3.SIF
SG5A
930
SG5B (uStr)
100
A3.SIF
SG5B
930
SG5_TAIV (uStr)
110
A3.SIF
SG5_TAIV
140
Time (secs)
3000

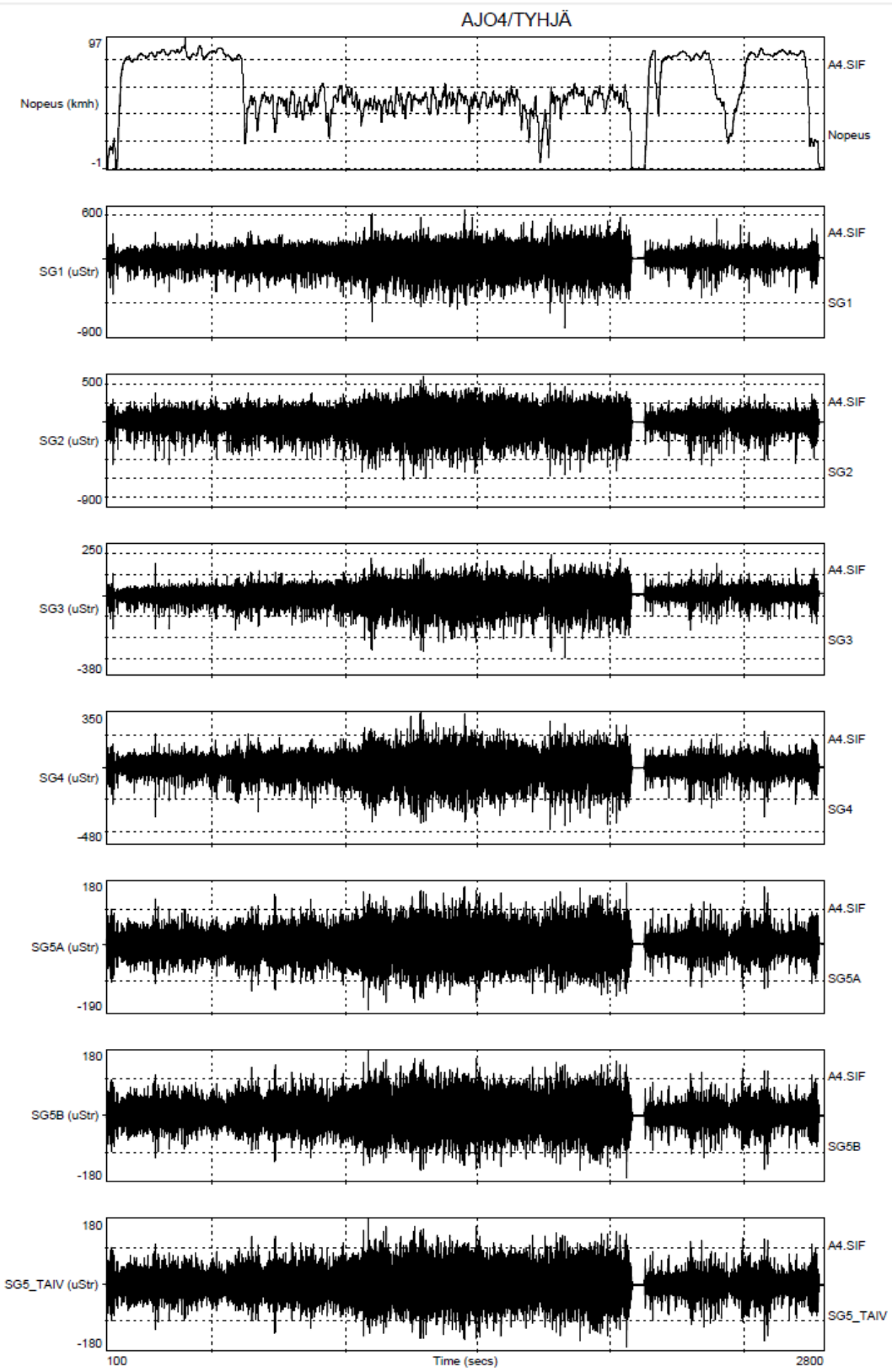
AJO4/TYHJÄ
97
Nopeus (kmh)
-1
A4.SIF
Nopeus
600
SG1 (uStr)
-900
A4.SIF
SG1
500
SG2 (uStr)
-900
A4.SIF
SG2
250
SG3 (uStr)
-380
A4.SIF
SG3
350
SG4 (uStr)
-480
A4.SIF
SG4
180
SG5A (uStr)
-190
A4.SIF
SG5A
180
SG5B (uStr)
-180
A4.SIF
SG5B
180
SG5_TAIV (uStr)
-180
A4.SIF
SG5_TAIV
100
Time (secs)
2800

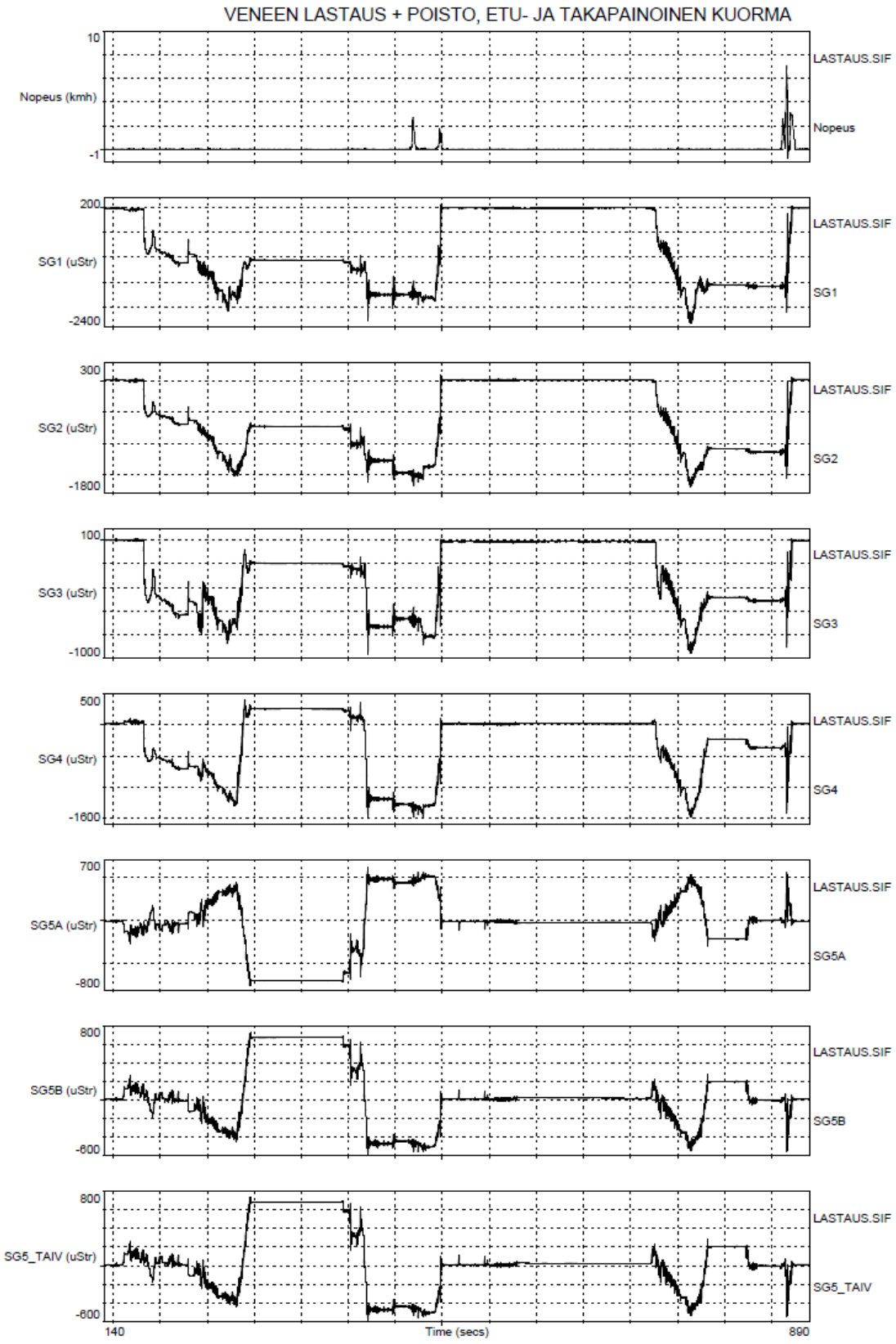
VENEEN LASTAUS + POISTO, ETU- JA TAKAPAINOINEN KUORMA
10
Nopeus (kmh)
-1
LASTAUS.SIF
Nopeus
200
SG1 (uStr)
-2400
LASTAUS.SIF
SG1
300
SG2 (uStr)
-1800
LASTAUS.SIF
SG2
100
SG3 (uStr)
-1000
LASTAUS.SIF
SG3
500
SG4 (uStr)
-1600
LASTAUS.SIF
SG4
700
SG5A (uStr)
-800
LASTAUS.SIF
SG5A
800
SG5B (uStr)
-600
LASTAUS.SIF
SG5B
800
SG5_TAIV (uStr)
-600
LASTAUS.SIF
SG5_TAIV
140
Time (secs)
890

ANALYTICAL CALCULATIONS FOR S420 TRAILER

Reaction force calculations

An example of trailer hitch reaction force calculation for flat load case:

W_k is the section modulus of the shaft, σ_m is the bending stress from the strain gage measurement results, *Na* is the reaction force at the trailer hitch and *l* is the distance of the strain gages 5a and 5b from the trailer hitch.

$$Mc = W_k * \sigma_m$$

$$Mc = 17{,}51 * 10^3 * 58$$

$$Mc = 998\ Nm$$

$$N_a = \frac{M_c}{l}$$

$$Na = \frac{998}{2.14} = \mathbf{466}\ N$$

According to calculated reaction forces for all load cases, the correct loading is set to FEA-models. Same kind of calculations is made for all of the static load cases.

Buckling and bending calculations

According to the strain gage measurement results, the axial stresses are not critical for the structure. The greatest axial stresses are the size of 10 MPa, so the buckling effect is not critical. According to this information, only the bending calculations are made for the shaft.

The worst case for shaft's bending is the front-heavy load case. From the strain gage measurement data the real bending stress is used in the calculations.

From Ruukki's Rakenneputket-opus, the maximum allowed bending moment for 80x60x3 S420 N/mm^2 profile is 8.89 kNm.

$M_{Rd,1}$ = **8.89** kNm
I = 700500 mm^4
e = 40 mm
σ_m = (SG5a-SG5b)/2 = (-92.7-90.3)/2 = 91.5 MPa

$$M_{Ed,1} = \frac{I * \sigma_m}{e}$$

$$M_{Ed,1} = \mathbf{1.6}\ kNm$$

$$M_{Rd,1} > M_{Ed,1}, \quad OK$$

Calculations are made also with dynamic amplification factor, which is calculated from the data of obstacle overrun for both of the tires.
$\Delta\sigma_{dynamic}$=430 MPa
$\Delta\sigma_{static}$=91.5 MPa

$$DAF = \frac{\Delta\sigma_{dynamic}}{\Delta\sigma_{static}}$$

$$DAF = 4.7$$

$$M_{Ed,1,DAF} = \frac{I * \sigma_m * DAF}{e}$$

$$M_{Ed,1,DAF} = \mathbf{7.52}\ kNm$$

$$M_{Rd,1} > M_{Ed,1,DAF} \quad OK$$

Lateral buckling

Lateral-torsional buckling does not reduce the bending durability, if slenderness fills the condition: $\lambda_{LT} < \lambda_{LT.0} = 0.4$. (Ruukki, 2012, p. 86) The calculations are performed to shaft, where the loading is assumed to be nodal load in the center of the shaft. If the shaft withstands this loading, it withstands in the trailer.

$C_1 = 1.365$
$C_2 = 0.553$
$k = 1.0$
$L = 5300$ mm
$I_z = 44.89*10^4$ mm^4
$I_t = 88.35*10^4$ mm^4
$Z_g = 40$ mm
$G = 82\,000$ MPa

$$M_{cr,1} = C_1 \frac{\pi^2 E I_z}{(kL)^2} \left[\sqrt{\frac{(kL)^2 G I_t}{\pi^2 E I_z} + (C_z Z_g)^2} - (C_z Z_g) \right]$$

$$M_{cr,1} = 65\ kN\text{m}$$

$$\lambda_{LT} = \sqrt{\frac{W_y f_y}{M_{cr,1}}}$$

$$\lambda_{LT} = 0.333$$

$$\lambda_{LT} = 0.333 < \lambda_{LT.0} = 0.4 \qquad \text{OK}$$

Local buckling

Material S420

Cross section class 3

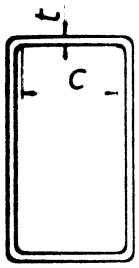

Profiles: 80x60x3

Ψ = 1

ε = 0.748

Condition: $\frac{c}{t} < 42 * \varepsilon$

Shaft: $\frac{c}{t} = \frac{54}{3} = 18 < 31{,}4 \quad OK$

Cross section class 4

Profile: 80x60x3

Ψ = 1 $k_\sigma = 4$

$$\sigma_{cr,p} = \frac{k_c * 190000}{\left(\frac{c}{t}\right)^2} = 2345.7$$

$$\lambda_p = \sqrt{\frac{fy}{c_{cr,p}} = 0.4232}$$

$$\rho = \frac{\lambda_p - 0.055*(3+\psi)}{\lambda_p^2} = 1.1345 = 1.0$$

ε = 0.748

Condition: $\frac{c}{t} < 38{,}3 * \varepsilon$

Shaft: $\frac{c}{t} = \frac{54}{3} = 18 < 28.6 \quad OK$

ANALYTICAL CALCULATIONS FOR TRAILER WITH FORM 800

Buckling and bending calculations

Same kind of calculations as for the current trailer is performed for the Form 800 geometry. Now the shafts profile is 80x60x2. The design value according to bending moment:

Condition: $M_{Rd,2} > M_{Ed,2}$

$I = 5.114*10^5$

$f_y = 600$ MPa

$\gamma_{M0} = 1.0$

$$M_{Rd,2} = \frac{W_y f_y}{\gamma_{M0}}$$

$$W_y = \frac{BH^3 - bh^3}{6H}$$

$$W_y = 12\,786\ mm^3$$

$$M_{Rd,2} = \mathbf{7.67\ kNm}$$

$$M_{Ed,2} = \frac{I * \sigma_m}{e}$$

$$M_{Ed,2} = \mathbf{1.7\ kNm}$$

$$M_{Rd,2} > M_{Ed,2} \quad OK$$

Calculations are made also with dynamic amplification factor, which is calculated from the obstacle overrun for both of the tires data.

$\Delta\sigma_{dynamic}$=430 MPa

$\Delta\sigma_{static}$=91,5 MPa

$$DAF = \frac{\Delta\sigma_{dynamic}}{\Delta\sigma_{static}}$$

$$DAF = 4.7$$

$$M_{Ed,2,DAF} = \frac{I * \sigma_m * DAF}{e}$$

$$M_{Ed,2,DAF} = \mathbf{5.5}\ kNm$$

$$M_{Rd,2} > M_{Ed,2,DAF}, \quad OK$$

Lateral buckling

$C_1 = 1.365$

$C_2 = 0.553$

k = 1.0

L = 5300 mm

$I_z = 32.8*10^4$ mm^4

$I_t = 59.5*10^4$ mm^4

$Z_g = 40$ mm

G = 82 000 MPa

$W_y = 12.8*10^3$ mm^3

f_y = 600 MPa

$\Phi_{LT} = 0.568$

$$M_{cr,2} = C_1 \frac{\pi^2 E I_z}{(kL)^2}\left[\sqrt{\frac{(kL)^2 G I_t}{\pi^2 E I_z} + (C_z Z_g)^2} - (C_z Z_g)\right]$$

$$M_{cr,2} = 46\ kNm$$

$$\lambda_{LT} = \sqrt{\frac{W_y f_y}{M_{cr,2}}}$$

$$\lambda_{LT} = 0.416$$

$\lambda_{LT} = 0.416 < \lambda_{LT.0} = 0.4$ NOT OK

Closer examination:

$$\chi_{LT} = \frac{1}{\Phi_{LT} + \sqrt{\Phi_{LT}^2 - \beta\lambda_{LT}^2}}$$

$$\chi_{LT} = 0.993$$

$$M_{Rd,3} = W_y \frac{\chi_{LT} f_y}{\gamma_{M1}}$$

$$M_{Rd,3} = 6.9\ kNm$$

$$M_{Rd,3} > M_{Ed,2} \quad OK$$
$$M_{Rd,3} > M_{Ed,2,DAF} \quad OK$$

Local buckling

Material Form 800

Cross section class 3

Profile: 80x60x2

Ψ = 1

ε = 0.626

Condition: $\frac{c}{t} < 42 * \varepsilon$

Shaft: $\frac{c}{t} = \frac{56}{2} = 28 > 26{,}3 \quad NOT\ OK$

Cross section class 4

Profile: 80x60x2

Ψ = 1 $k_\sigma = 4$

$$\sigma_{cr,p} = \frac{k_c * 190000}{\left(\frac{c}{t}\right)^2} = 2345.7$$

$$\lambda_p = \sqrt{\frac{fy}{c_{cr,p}}} = 0.4232$$

$$\rho = \frac{\lambda_p - 0.055*(3+\psi)}{\lambda_p^2} = 1.1345 = 1.0$$

ε = 0.626

Condition: $\frac{c}{t} < 38{,}3 * \varepsilon$

Shaft: $\frac{c}{t} = \frac{54}{2} = 18 < 24 \quad OK$

If the profile of the shaft is changed to 90x50x2

Cross section class 3

Ψ = 1

ε = 0.626

Condition: $\frac{c}{t} < 42 * \varepsilon$

Shaft: $\frac{c}{t} = \frac{46}{2} = 23 < 26{,}3 \quad OK$

FATIGUE LIFE CALCULATIONS

Current trailer

Example of fatigue life calculation:

FAT=630

m=3

$\Delta\sigma_{eqv}$= From the notch rounding of FE-model

$$N = (\frac{FAT}{\Delta\sigma_{eqv}})^m * 2 * 10^6$$

Tarmac, flat load:

$$N_f = \left[\frac{630}{7300}\right]^3 * 2 * 10^6$$

$$N_f = 1286$$

Test drive route was 23,5 km long.

$$\underline{N_f = 1286 * 23.5 = 30\ 200\ km}$$

Gravel, flat load:

$$N_f = \left[\frac{630}{12000}\right]^3 * 2 * 10^6$$

$$N_f = 290$$

Test drive route was 20 km long.

$$\underline{N_f = 290 * 20 = 5\ 800\ km}$$